U.S.N.A. --- Trident Scholar project report; no. 301 (2002)

OPTICAL LIMITING WITHIN CAPILLARY WAVEGUIDES

by

Midshipman Jeremiah J. Wathen, Class of 2002
United States Naval Academy
Annapolis, Maryland

_____

Certificate of Advisor(s) Approval

Assistant Professor James J. Butler
Physics Department

_____

_____

Acceptance for the Trident Scholar Committee

Professor Joyce E. Shade
Deputy Director of Research & Scholarship

_____

_____

REPORT DOCUMENTATION PAGE

Form Approved OMB No. 0704-0188

1. REPORT DATE (DD-MM-YYYY) 07-05-2002	2. REPORT TYPE	3. DATES COVERED (FROM - TO) xx-xx-2002 to xx-xx-2002

4. TITLE AND SUBTITLE
Optical Limiting Within Capillary Waveguides
Unclassified

5a. CONTRACT NUMBER
5b. GRANT NUMBER
5c. PROGRAM ELEMENT NUMBER

6. AUTHOR(S)
Wathen, Jeremiah J. ;

5d. PROJECT NUMBER
5e. TASK NUMBER
5f. WORK UNIT NUMBER

7. PERFORMING ORGANIZATION NAME AND ADDRESS
U.S. Naval Academy
Annapolis, MD21402

8. PERFORMING ORGANIZATION REPORT NUMBER

9. SPONSORING/MONITORING AGENCY NAME AND ADDRESS
,

10. SPONSOR/MONITOR'S ACRONYM(S)

11. SPONSOR/MONITOR'S REPORT NUMBER(S)

12. DISTRIBUTION/AVAILABILITY STATEMENT
APUBLIC RELEASE
,

13. SUPPLEMENTARY NOTES

14. ABSTRACT
See report.

15. SUBJECT TERMS

16. SECURITY CLASSIFICATION OF:			17. LIMITATION OF ABSTRACT Public Release	18. NUMBER OF PAGES 78	19. NAME OF RESPONSIBLE PERSON email from USNA, Annapolis, MD, (blank) lfenster@dtic.mil
a. REPORT Unclassified	b. ABSTRACT Unclassified	c. THIS PAGE Unclassified			19b. TELEPHONE NUMBER International Area Code Area Code Telephone Number 703767-9007 DSN 427-9007

Standard Form 298 (Rev. 8-98)
Prescribed by ANSI Std Z39.18

REPORT DOCUMENTATION PAGE		**Form Approved** **OMB No. 074-0188**

Public reporting burden for this collection of information is estimated to average 1 hour per response, including g the time for reviewing instructions, searching existing data sources, gathering and maintaining the data needed, and completing and reviewing the collection of information. Send comments regarding this burden estimate or any other aspect of the collection of information, including suggestions for reducing this burden to Washington Headquarters Services, Directorate for Information Operations and Reports, 1215 Jefferson Davis Highway, Suite 1204, Arlington, VA 22202-4302, and to the Office of Management and Budget, Paperwork Reduction Project (0704-0188), Washington, DC 20503.

1. AGENCY USE ONLY (Leave blank)	2. REPORT DATE 7 May 2002	3. REPORT TYPE AND DATE COVERED	
4. TITLE AND SUBTITLE Optical limiting within capillary waveguides		5. FUNDING NUMBERS	
6. AUTHOR(S) Wathen, Jeremiah J. (Jeremiah Joseph), 1980-			
7. PERFORMING ORGANIZATION NAME(S) AND ADDRESS(ES)		8. PERFORMING ORGANIZATION REPORT NUMBER	
9. SPONSORING/MONITORING AGENCY NAME(S) AND ADDRESS(ES) US Naval Academy Annapolis, MD 21402		10. SPONSORING/MONITORING AGENCY REPORT NUMBER Trident Scholar project report no. 301 (2002)	
11. SUPPLEMENTARY NOTES			
12a. DISTRIBUTION/AVAILABILITY STATEMENT This document has been approved for public release; its distribution is UNLIMITED.			12b. DISTRIBUTION CODE

13. ABSTRACT: A study of the optical limiting characteristics of capillary waveguides containing highly nonlinear cores is reported. Nonlinear waveguides prove useful, both for the study of fundamental physical phenomena they display and for practical applications (such as optical limiting) they may fulfill. Work presented here strives to use nonlinear waveguides as optical limiting elements, incorporating the waveguides into geometries that may integrate into modern optical fiber systems. Multi-mode and single-mode nonlinear waveguides, with core diameters ranging from 3.2 to 200 μm, were filled with solutions of silicon naphthalocyanine (SiNc). SiNc displays large absorptive and refractive index nonlinearity. The transmission characteristics of these nonlinear waveguides were measured as a function of incident energy from two different pulsed, frequency-doubled Nd:YAG lasers (producing 7 ns and 5 ns pulses at 532 nm). For the multimode waveguides, nonlinear effects are observed at input energies as low as 1.0×10^{-10} J and a transmission of 5% or less was observed for input energies as low as 1.0×10^{-7} J. For the single-mode waveguide, a limiting response was stimulated at input pulse energies < 20 pJ. Multi-mode waveguide data were compared with a three-level sequential absorption model, which modeled the nonlinear behavior of SiNc.
.

14. SUBJECT TERMS: **nonlinear, limiting, capillary waveguide, reverse-saturable absorption**		15. NUMBER OF PAGES 78	
		16. PRICE CODE	

17. SECURITY CLASSIFICATION OF REPORT	18. SECURITY CLASSIFICATION OF THIS PAGE	19. SECURITY CLASSIFICATION OF ABSTRACT	20. LIMITATION OF ABSTRACT

Abstract

A study of the optical limiting characteristics of capillary waveguides containing highly nonlinear cores is reported. Nonlinear waveguides prove useful, both for the study of fundamental physical phenomena they display and for practical applications (such as optical limiting) they may fulfill. Work presented here strives to use nonlinear waveguides as optical limiting elements, incorporating the waveguides into geometries that may integrate into modern optical fiber systems.

Multi-mode and single-mode nonlinear waveguides, with core diameters ranging from 3.2 to 200 μm, were filled with solutions of silicon naphthalocyanine (SiNc). SiNc displays large absorptive and refractive index nonlinearity. The transmission characteristics of these nonlinear waveguides were measured as a function of incident energy from two different pulsed, frequency-doubled Nd:YAG lasers (producing 7 ns and 5 ns pulses at 532 nm). For the multimode waveguides, nonlinear effects are observed at input energies as low as 1.0×10^{-10} J and a transmission of 5% or less was observed for input energies as low as 1.0×10^{-7} J. For the single-mode waveguide, a limiting response was stimulated at input pulse energies < 20 pJ.

Multi-mode waveguide data were compared with a three-level sequential absorption model, which modeled the nonlinear behavior of SiNc.

Keywords: nonlinear, limiting, capillary waveguide, reverse-saturable absorption

Acknowledgements

  First and foremost, I wish to extend my heartfelt love and thanks to my mother and father. Without their support, I would never have made it through the Naval Academy. Their care and understanding have made this project all the more enjoyable. Thank you, mom and dad, for everything.

  I also wish to show my gratitude to my advisor, Dr. James J. Butler. He has accommodated me in every way possible during this adventure into optics. Thank you, sir, for your commitment to this project, for the patience you demonstrated while I slowly learned the basics involved in running an optics lab, and for the friendship that we have built. I value your influence on my life and I look forward to spending much more time with you in the future.

  To my mentors at the Naval Research Laboratory, thank you as well. Jim Shirk, Richard Pong and Steve Flom have shown me what it means to work as a research scientist. I have seldom met such an eclectic and talented group of people. Thank you especially to Richard, for giving up lab space so we could experiment. Also, thanks for teaching me how to cook a turkey in a deep fryer.

  Thank you to my 11th Company shipmates, whose gentle chiding and good humor motivated me to give my all. As much as I look forward to 24 May 2002, I dread having our tightly knit tapestry of friends unwoven. To my roommates, I am sorry for the many nights I stayed up till the wee hours clicking away on the computer keyboard. I think you will see that it has paid off in the end.

  Finally, I hope the sun is shining bright on all my friends in Kentucky. I miss you and I look forward to seeing you again.

Contents

1. Introduction

An optical limiting element acts just as its name implies—an optical limiter controls the intensity of light transmitting through it. Such a device allows transmission of low intensity light, but denies transmission of high intensity light. In fact, a perfect optical limiter would be transparent against low intensities of light, but would very quickly become opaque when irradiated with high intensity light. Many applications demand optical limiters.[1] On the battlefield, protecting troops' eyes from exposure to intense laser light sources necessitates scope-sighting mechanisms that incorporate optical limiters operating against visible wavelengths. Also, fiber optical communications technology requires optical limiting elements that operate in the infrared spectrum; optical limiters can protect sensitive instruments utilized in fiber optic networks.

The above applications place rather challenging design parameters on an optical limiter. They demand nearly full transmission of low intensity light, but require limiting the transmitted fluence (energy density) to about $0.5\mu J/cm^2$ in order to prevent damage to protected instruments or eyes.[2] Furthermore, these applications require an optical limiter that can respond quickly (on the nanosecond timescale) in order to provide protection against short-pulsed laser light.[1] Practical electronic optical limiter designs prove incapable of responding on such a fast timescale. Finally, the widespread use of optical fibers in imaging and communications has led to the necessity for an optical limiter that can be readily integrated into optical fiber applications.

Nonlinear optical materials seem the best choice for optical limiting applications. These materials have optical properties—such as absorptive coefficients and indices of refraction—that depend strongly on the intensity of light incident upon them. Because of these intensity dependent properties, many nonlinear compounds can act as optical limiters. Some can do so

even against short-pulsed laser light—their optical properties change quickly enough to limit light within nano- or picoseconds of exposure.[3]

The Trident Project providing the basis for this report was an investigation into the limiting characteristics of silicon naphthalocyanine (a nonlinear optical material), when housed within the geometries of various optical fiber waveguides. Silicon naphthalocyanine (SiNc) is a well-studied nonlinear material,[4] but its limiting ability has never before been tested when housed within the core of an optical fiber waveguide. Specifically, this project was an endeavor to test SiNc in this new geometry. More broadly, the project sought to define the general characteristics of waveguides incorporating a wide variety of nonlinear materials.

To give some background, this report discusses mechanisms by which nonlinear materials (such as SiNc) can limit and provides the basic groundwork for optical fiber and mode theory. It gives an in-depth explanation of the investigated waveguide limiter design (which was devised as part of the project). This design meets many of the prerequisites demanded by applications. Furthermore, it provides the experimental setup and methodology used to study the design and it presents data harvested from the design. Finally, it compares the results of computerized limiter simulations to the actual data.

Presented findings shed light on a number of questions. Firstly, how effectively can SiNc-filled nonlinear waveguides limit against a range of input laser pulse energies? Secondly, how does limiting within the geometry of a waveguide differ from limiting in a free-space environment? Finally, how does the limiting capability of a single-mode waveguide limiter compare to the ability of a multi-mode waveguide limiter? To our knowledge, optical limiting within a single-mode waveguide has never before been seen. The results gained from the

investigated waveguides were truly encouraging and the limiting effects observed in some of the

test waveguides stand among the best limiting responses ever observed (see Figure 1).

Figure 1: Fractional transmission vs. energy input (per pulse) for a 10 μm diameter, 1.8 cm long, SiNc-filled waveguide optical limiter and for a simulated SiNc bulk-sample optical limiter. Black data points are the limiting response of a 10 μm nonlinear SiNc waveguide. The black line with triangles is a simulation of the limiting response for a bulk sample of SiNc. The graph indicates that a SiNc waveguide optical limiter is much more effective than a similar SiNc bulk-sample optical limiter.
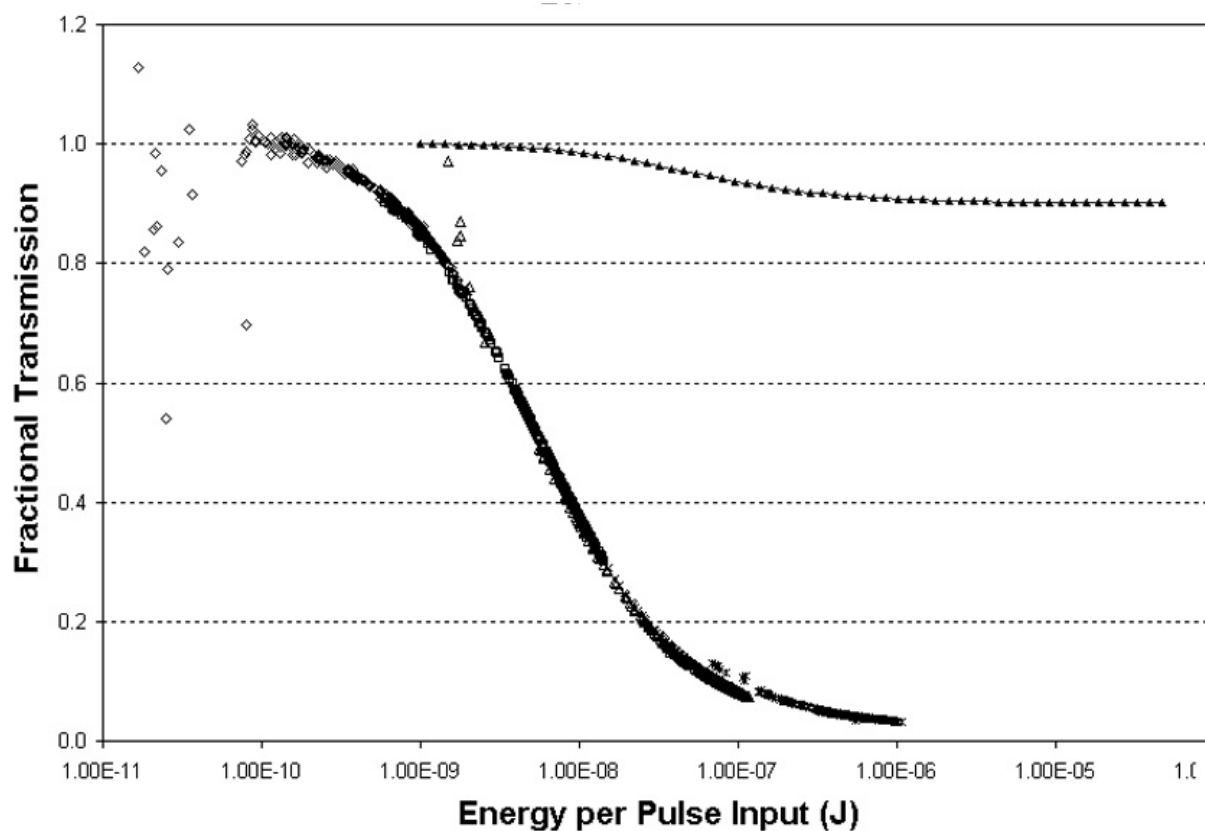
2. Background

A. Nonlinearity

Most familiar compounds are, for all intents and purposes, optically linear. Take a pane of window glass, for instance. A windowpane transmits the same percentage of light no matter how much sunshine hits it—this is the essence of a linear substance. If it is a sunny day outside, the window allows a lot of light into your home. If it is a cloudy day, the glass transmits less light into your home.

Materials used in this project are optically nonlinear. They exhibit nonlinearity with respect to coefficient of absorption, index of refraction, or with respect to both of these properties at once. But, what does it mean to say that a molecule's optical properties are nonlinear? To illustrate, first consider the property of light absorption.

1. Nonlinear Absorption

A material's coefficient of absorption is an empirically determined value that indicates how much light energy it can absorb when irradiated. Eqn. (1) is a common expression for a material's coefficient of absorption. This particular formulation is used when the material's absorptive coefficient displays intensity dependence (the coefficient of absorption for the material this project studied is actually fluence dependent. Eqn (1) is given here because it illustrates the nonlinear concept well). For a particular wavelength (or color) of light, α represents the absorption coefficient[2]

$$\alpha = \alpha_0 + \alpha_2 I. \tag{1}$$

Here, α_0 represents the material's linear coefficient of absorption. The linear coefficient displays no dependence upon I (the intensity of light hitting the material). Supposing that the material is optically linear against a range of light intensities, only α_0 significantly contributes to its overall

coefficient of absorption. However, if the material in question displays absorptive nonlinearity against a range of incident light intensities, then the term $\alpha_2 I$—the nonlinear absorption term—is sufficiently large to affect the overall expression of α. In the nonlinear case, as incident light intensity fluctuates, so does the material's overall coefficient of absorption. That is, as incident light intensity fluctuates, so does the material's ability to absorb light energy. A compound exhibiting a large, positive α_2 may prove suitable for use in the design of an optical limiter. The larger the light intensity incident upon such a compound, the more energy the compound will absorb.

Equation (1) is a linear equation with respect to the intensity of incident light. However, the fundamental equation that governs the propagation of light in a material is the wave equation. This equation deals with the electric field (or magnetic field) of the incident light. The intensity of an electromagnetic wave is related to the electric field by[5]

$$I = \frac{1}{2} c\varepsilon_0 E_0^2, \tag{2}$$

where c is the speed of light, ε_0 is the free space permittivity constant, and E_0 is the amplitude of the light wave's electric field. The coefficient of absorption relates to the light's electric field amplitude in a truly nonlinear relationship.

2. Nonlinearity in Index of Refraction

Also central to this project, a compound can display nonlinearity with respect to its index of refraction. A material's index of refraction, n, is a measure of the speed of light through the material

$$n = c/v, \tag{3}$$

where c is the speed of light in a vacuum and v is the speed of light through the medium. Similar to the expression of the absorptive coefficient, a compound's index of refraction is given by[2]

$$n = n_0 + n_2I. \qquad\qquad\qquad (4)$$

For a substance displaying a nonlinear index of refraction, the factor n_2 has a large magnitude. As incident light intensity fluctuates, such a compound's index of refraction will change. It will become apparent later (in discussion of total internal reflection) that certain compounds, having $n_2 \ll 0$, can act as limiters when incorporated into the core of optical fiber waveguides.

B. Nonlinear Mechanisms

1. Nonlinear Absorption Mechanisms

When irradiated by wavelengths in the visible spectrum and through the infrared, molecules use electronic transitions to absorb and re-radiate light energy. If an energetic photon hits a low-energy electron (which is bound by the attractive forces of a molecule's nuclei), the electron can absorb the photon's energy and transit to an excited state (in which the electron is still bound by the nuclei, but in a less stable energetic state). For simple transitions, this excited state will typically decay very quickly ($\sim 10^{-8}$ seconds),[6] and the electron will transit down to its initial ground state. Usually, the emission of a photon, equal in energy to the photon that stimulated the absorption process in the first place, will accompany the de-excitation and pass out of the molecule. This bucket brigade model provides a simple explanation as to how light traverses through different media.

However, for some electronic processes, the lifetime of a stimulated electron's excited state endures so long that the excited electron dissipates its energy via mechanisms other than the generation of a photon (for instance, through thermal dissipation). In this case, the electron will absorb the incident photon, but it will not emit a photon upon de-excitation. In such processes, the transiting electron converts the incident light energy into another form of energy. Such non-radiating processes determine a material's absorptive coefficient.

A few types of electronic absorption processes lend themselves to creating nonlinear absorptive abilities against relatively low-intensity radiation, among them two-photon absorption (TPA) and reverse-saturable absorption (RSA). Electronic processes can occur extremely quickly (sometimes within femtoseconds of exposure to light radiation), and processes like TPA and RSA provide the most promise for creating a limiting response against very short-pulsed laser light sources.

a) Two-Photon Absorption

In a molecule that displays two-photon absorption, an electron cannot absorb the energy from simply one photon of wavelength λ. The energy associated with one photon (wavelength λ) is too low to boost the electron to its excited state. However, for these special molecules, a single electron can absorb two photons' (each of wavelength λ) energies *simultaneously* in order to transit to its excited state.

Figure 2 is a very simple molecular energy diagram that depicts a TPA process. L_0 is the molecule's low-energy ground state and L_1 is its excited state. In order for TPA to occur, two photons must strike the same electron residing in state L_0 at nearly the same moment. Each of these photons carries energy E, where $E = hc/\lambda = h\nu$ (h is Planck's constant, c is the speed of light, λ is the wavelength of the photon, ν is the frequency of the photon). Upon absorbing the energy associated with the two photons, the electron transits to state L_1, which lies above L_0 by an amount 2E.

Figure 2: A molecular energy schematic depicting TPA.

This process is highly improbable—it's just not very likely that two photons will simultaneously strike an electron. Against low incident light intensities, when relatively few photons strike the TPA molecule per unit time, TPA events remain virtually nonexistent. However, under more intense radiation, the raw increase in the number of bombarding photons per unit time increases the likelihood of TPA. Higher incident intensities provoke more and more TPA events, markedly increasing the molecule's ability to absorb energy. TPA is a nonlinear, intensity dependent effect.

b) Reverse-Saturable Absorption

TPA has a close relative in the phenomenon called reverse-saturable absorption (RSA). While TPA causes one electron to simultaneously absorb the energy of two photons, RSA involves a single electron making two separate absorptions. Consider a molecule whose electron energy states are described by the simplified energy schematic of Figure 3. For an electron residing in level L_0, the ground-state absorption cross section, σ_g, indicates the probability that it will excite to level L_1 and absorb a photon's energy. Likewise, for an electron in energy level L_1, the excited-state absorption cross section, σ_e, indicates the probability that the electron will excite to level L_2 and absorb a photon's energy.

Figure 3: An RSA molecule's energy diagram.
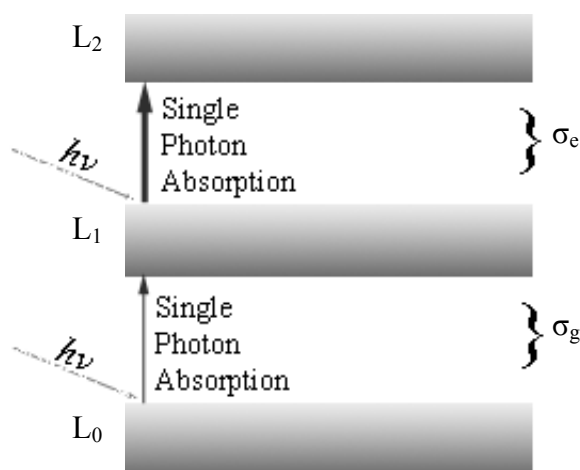
In an RSA-prone molecule, σ_e is much greater than σ_g. That is, once level L_1 is significantly populated, it is more likely for an electron to transit from L_1 to L_2, than from L_0 to L_1.

For an RSA molecule facing relatively low-intensity radiation, state L_1

will not gain a significant population of electrons. The molecule's absorptive ability will be determined by electron transitions between L_0 and L_1. However, as the intensity of the incident light increases, a significant number of electrons will populate L_1, and electron excitations to L_2 will become possible. Because $\sigma_e > \sigma_g$, once electrons in L_1 begin exciting to L_2, the reverse-saturable absorber's ability to absorb light energy increases. This is in contrast to the more common saturable absorber, in which $\sigma_g < \sigma_e$. In the saturable absorber, the saturation *decreases* as the intensity becomes greater since the electrons in the excited state (L_1) are less prone to absorb additional photons.

2. Relating Cross Section and Absorptive Coefficient for an RSA Solution

Understanding the mathematical expressions relating a molecule's absorption cross sections to its coinciding absorptive coefficient proves important when trying to model the behavior of reverse-saturable absorbers. To this point, absorption cross sections and absorptive coefficients have been discussed as separate entities, but they directly relate to one another.

The nonlinear material investigated in this project, silicon naphthalocyanine (SiNc), is a reverse-saturable absorber. However, the simple expression for a coefficient of absorption outlined by eqn. (1) cannot apply to a solution of SiNc molecules. Eqn. (1) applies to intensity dependent reverse-saturable absorption. In the experiments presented later, SiNc responds to input pulses of light in a fluence dependent manner (that is, SiNc's nonlinear response depends upon the total amount of energy per area $[J/m^2]$ an incident pulse delivers, rather than on the intensity $[W/m^2]$ the incident pulse exhibits). Thus, the expression soon given (in eqn. (7)) for the coefficient of absorption appears different than the expression in eqn. (1).

SiNc molecules approximately conform to a three-level RSA model (like the one in Figure 3). When light irradiates a solution of SiNc, some fraction of the dissolved SiNc

molecules absorb light and become excited; in these excited molecules, state L_1 gains a significant electron population. The rest of the SiNc molecules in solution remain unexcited; state L_1 remains unpopulated for these ground-state molecules. These two groups of SiNc molecules, the ground-state group and the excited group, each contribute to the overall absorptive ability of the solution differently (because $\sigma_e > \sigma_g$). In determining a solution's coefficient of absorption, the absorptive affect created by each of these groups must be treated separately.

The ground-state coefficient of absorption, α_g, derives from the ground-state group of SiNc molecules through the relationship[3]

$$\alpha_g = (\sigma_g)(C_1)(N_A)\left(\frac{1\,L}{1000\,mL}\right). \qquad (5)$$

Here, C_1 stands for the molar concentration [mol/L] of the unexcited RSA molecules in solution. N_A is Avogadro's Number.

Likewise, α_e, the RSA solution's excited-state absorptive coefficient, derives from the excited-state group of SiNc molecules by[3]

$$\alpha_e = (\sigma_e)(C_2)(N_A)\left(\frac{1\,L}{1000\,mL}\right). \qquad (6)$$

C_2 represents the molar concentration [mol/L] of excited RSA molecules in solution.

For the RSA solution, then, the overall absorptive coefficient, α, is a conglomeration of the ground-state and excited-state coefficients, where

$$\alpha = \alpha_g + \alpha_e. \qquad (7)$$

As light energy incident upon a solution of SiNc molecules increases, the proportion of excited-state to unexcited-state molecules will shift in favor of the excited molecules. Thus, α_e will increasingly dominate over α_g in the expression of α. It is this shifting effect that causes

nonlinearity in SiNc's absorptive ability. There is a limit to SiNc's nonlinearity, though. Beyond a certain threshold of incident fluence, virtually all of the SiNc molecules in solution will enter the excited state. Thus, only the excited-state cross section will contribute to the solution's absorptive ability. Beyond this threshold fluence, the solution will again become optically linear (with respect to absorption) and $\alpha \sim \alpha_e$.

3. Nonlinear Mechanisms Affecting Refractive Index

The mechanisms producing the largest nonlinear changes in a compound's index of refraction are typically thermal in nature. In an irradiated compound, thermal changes arise due to various non-radiating intra- and intermolecular electron relaxations that follow linear and nonlinear photon absorptions. In short, under highly intense light, frequent photon absorptions produce local heating within an irradiated material. As the temperature of the irradiated system increases, the material will expand and decrease in density. The index of refraction of a substance depends on its density and, for most materials, a decrease in density leads to a decrease in index of refraction.[4] Therefore, by definition, most nonlinear absorbers also demonstrate nonlinearity in index of refraction.

C. Circular Optical Waveguide Theory

1. Why the Optical Waveguide?

In most previous investigations of nonlinear optical limiters, a nonlinear sample's limiting response is stimulated when light, focused by a lens, propagates into a freestanding sample of the material.[3] The rationale behind this setup makes sense. The lens, by focusing incident light, increases the intensity of the light to a maximum at its focal plane. For the irradiated sample, this increase in incident light intensity translates into a more marked nonlinear limiting response (remember, a nonlinear response depends upon light intensity). However, the

lens can only keep light tightly focused over a small region about its focal point—the Rayleigh

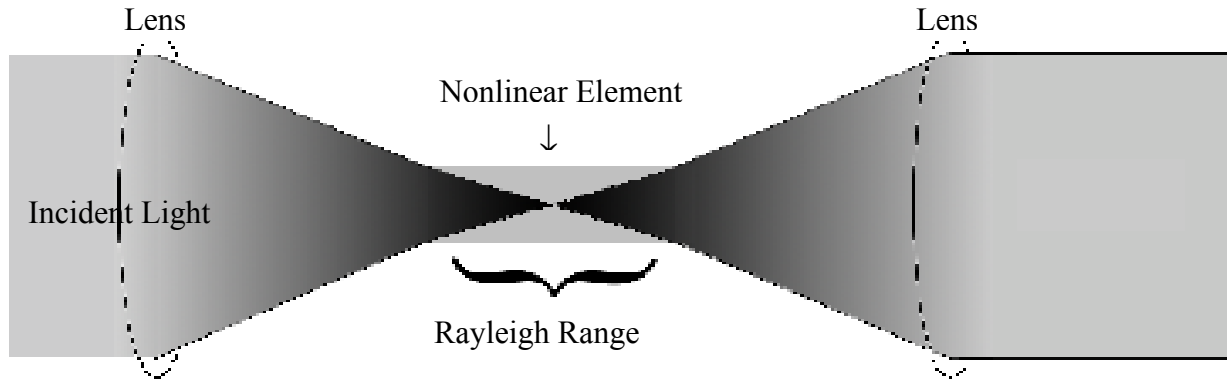Range (see Figure 4).[7] For a sample that requires very intense light to stimulate a nonlinear

Figure 4: A depiction of the traditional optical limiting experimental setup. The nonlinear element's ability to limit light is restricted by the spatial dimensions of the Rayleigh Range.

response, effective optical limiting will only occur within the confines of the Rayleigh Range.

Given the limiting abilities of many known nonlinear materials, a limiting response sufficient to

satisfy applications is difficult to achieve in this limited space.

The physical conditions present within the geometry of an optical waveguide provide a

much better limiting environment. Light must be focused into a waveguide by a lens. However,

in contrast to the freestanding sample design, a waveguide traps the focused light within its core.

Focused light travels through the waveguide's core in an intense beam, maintaining the high

intensity achieved at the lens's focal point. In effect, a waveguide can indeterminately extend

the Rayleigh Range.

Consider a waveguide whose core is composed of nonlinear limiting material. If light is

focused into the waveguide, it will remain intense, stimulating a nonlinear limiting response over

the entire length of the waveguide (or until the limiting material absorbs enough of the incident

light energy to kill its own nonlinear response). Waveguide limiter designs presented in this

report take advantage of this light-trapping property. As such, an understanding of fundamental

optical waveguide theory is crucial to an understanding of the designs presented.

2. Total Internal Reflection

Figure 5: The transmission and reflection of an incident ray according to Snell's Law.

$\theta_i = \theta_r > \theta_t$
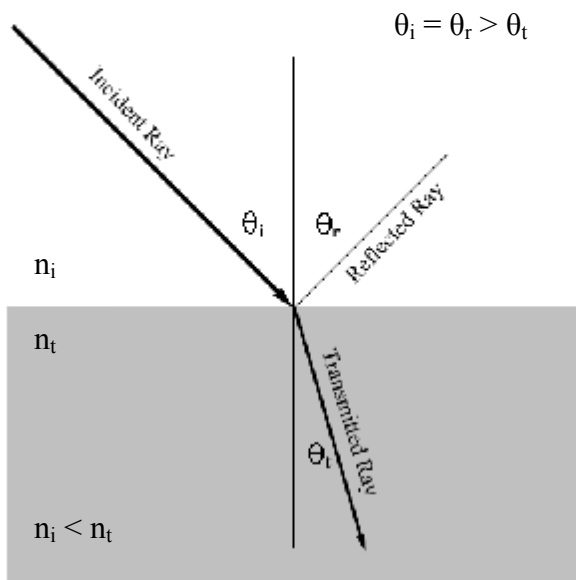
Fiber optical waveguides operate on the classically defined principle of total internal reflection, an interesting result of Snell's Law,[8]

$$n_i \sin \theta_i = n_t \sin \theta_t. \qquad (8)$$

As shown in Figure 5, light rays traveling across an interface from a medium of low refractive index, n_i, to a medium of high index, n_t, will bend toward the normal vector describing the interface's plane of tangency. Conversely, when light travels across an interface from a high refractive index to a lower refractive index, the incident light rays

bend away from the normal at the interface. In the latter case, when light rays strike the interface

at incident angles larger that a certain critical angle, they bend so sharply away from the normal

that they reflect rather than refract. Such rays are trapped in the medium of high refractive

index. The critical angle, θ_c, is derived from Snell's Law: $\theta_c = \sin^{-1}(n_t/n_i)$.[8] This light-trapping

phenomenon has been dubbed total internal reflection (TIR).

To take advantage of TIR, step-index optical fibers (waveguides) consist of a high-

refractive index core and a surrounding low-refractive index cladding. When light passes into

one end of the fiber with the proper orientation (i.e. an incident ray hits the core-cladding

interface at an angle greater than the critical angle—see Figure 6), the ray is guided within the

boundaries of the fiber core. The fiber will only support TIR for rays entering the end of the core

Figure 6: The trapping of a light ray within the core of a waveguide—total internal reflection.
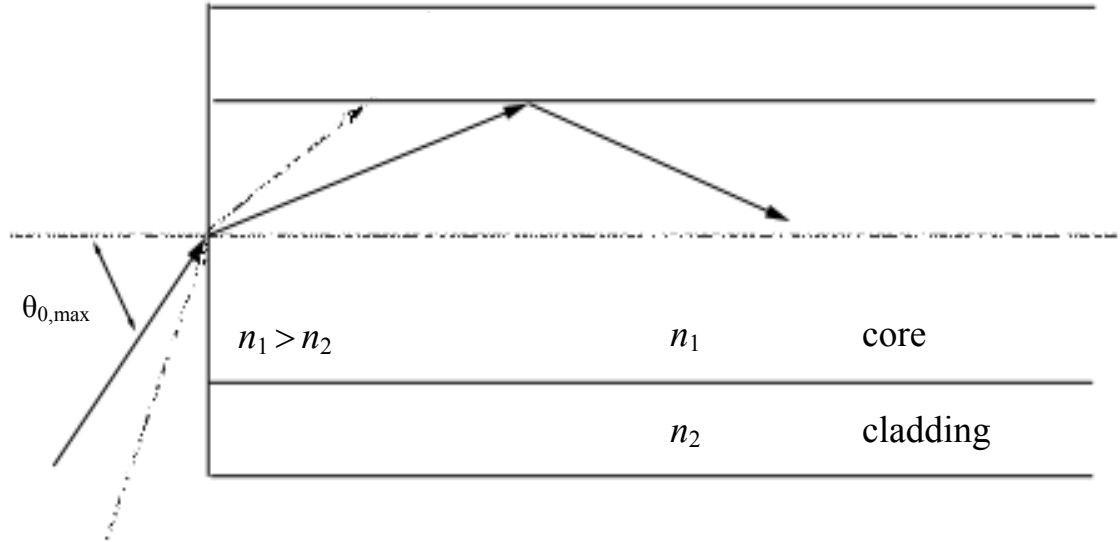
at an angle less than $\theta_{0,max}$, given by:[9]

$$\sin \theta_{0,\,max} = (n_1{}^2 - n_2{}^2)^{1/2} \, . \tag{9}$$

If a waveguide's core refractive index ever decreases below its cladding refractive index (this

can occur within nonlinear waveguides), the waveguide will no longer guide light within its core.

While most commercially available step-index optical fibers have solid cores, the core

need not be solid. Nonlinear waveguides discussed in this report consist of a small glass tube

(called a capillary) filled with a liquid solution of nonlinear molecules. For such a waveguide,

the high-refractive index nonlinear solution forms the waveguide's core and the glass capillary

acts as the waveguide's cladding. The nonlinear response of a waveguide's liquid core can be

deduced by testing its transmission efficiency against a range of different input light intensities.

3. Mode Theory for Circular Waveguides

a) What is a Mode?

The simple ray model presented above cannot completely describe the propagation of light guided within an optical fiber's core. Light guided within a waveguide's core must satisfy Maxwell's Equations and the electric and magnetic boundary conditions present at the waveguide's core-cladding interface. Having solved Maxwell's Equations given these conditions, it becomes evident that the electric and magnetic field distributions guiding along an optical fiber can be represented by a superposed set of bound modes. In a sense, each mode belonging to this set is an allowable pathway on which light can travel through the fiber.

Each guided mode propagates with a distinct electromagnetic field distribution (see Figure 7—these distributions can be described by Bessel Functions) that forms a standing wave
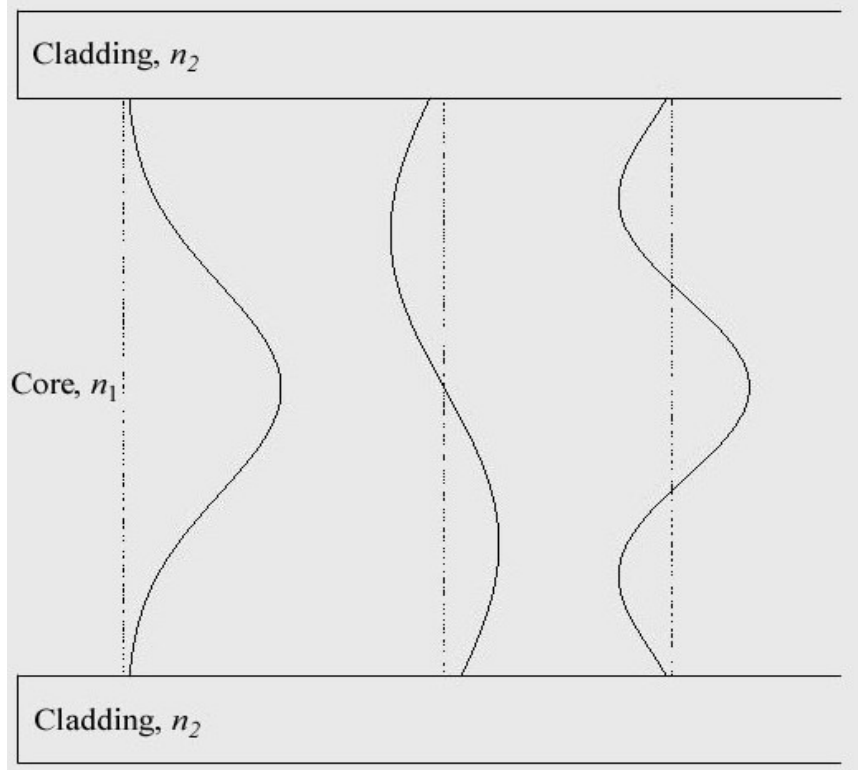
Figure 7: Some low order modes within a 2-D waveguide. While the text refers to 3-D circular waveguides, this picture helps present the concept of what a mode is. Each curve represents the electric field distribution for a different mode. The left-hand curve is the lowest order mode (the zero-order mode). A waveguide that only allows propagation of the lowest order mode is called a single-mode waveguide.

pattern, which begins at the core's transmission axis (the z-axis) and extends radially outward.

Depending upon a fiber's characteristics, it may permit few or many modes (a single-mode energy distribution pattern is depicted in Figure 8). Light energy focused into a fiber's core will distribute across the fiber's modal field and each mode will carry a fraction of the traversing light energy. In addition, as the light traverses, the modes may share energy amongst one another—the fraction of light energy each mode carries may change as the light propagates. Energy sharing among modes can drastically alter the cross-sectional energy distribution within a fiber's core as light propagates through it. This property of energy distribution and redistribution among a fiber's modes has implications for optical limiting within a fiber's core. These implications will be discussed in more depth later in the presentation of the single-mode limiter apparatus.
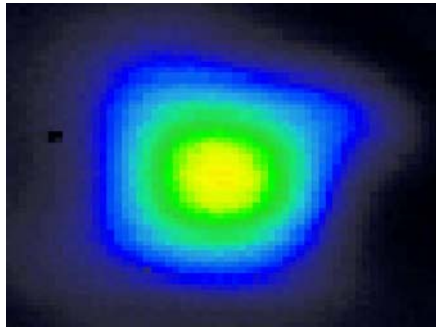
Figure 8: the energy distribution associated with the 0-order mode, the simplest of modes. This cross sectional image comes from the core of a fiber waveguide (the core is 2 μm in diameter). Yellow denotes the area of highest energy concentration and blue denotes the area of lowest concentration. The energy distribution is roughly circularly symmetric and Gaussian in the radial direction. A single-mode fiber can only allow this energy distribution to propagate.

b) Finding Allowed Modes

For monochromatic light of radian frequency w, a mode traveling in the positive z-direction (along a fiber's transmission axis) has a time and z dependence given by[9]

$$e^{i(wt - \beta z)}. \tag{10}$$

Here, β is the z-component of the wave propagation vector. A waveguide supports guided modes when,[9]

$$n_2 k < \beta < n_1 k, \tag{11}$$

where n_1 and n_2 are the refractive indices of the core and cladding, respectively. Also, k is the

free-space propagation constant given by k = $2\pi/\lambda$, where λ is the wavelength of the guided light.

Each possible mode corresponds to a different value of β; if a mode corresponds to a β outside

the bounds of eqn. (11), that mode will leak out of the core and its transmission will be lost.

Thus, relationship (11) is known as the cutoff condition. Because of the boundary conditions at

the core-cladding interface, β can assume only certain discrete values within the range prescribed

by eqn. (11).

Because each mode corresponds to a separate value of β, then each guided mode

experiences a slightly different index of refraction within the core, called n_{eff}. Therefore, we can

express the propagation constant of each guided mode as $\beta = n_{eff}k$. In this relationship, n_{eff} takes

on discrete values between n_1 and n_2.

Consider Maxwell's Equations for a linear, isotropic dielectric material having no

currents or free charges (such as the materials in a fiber):

$$\nabla \times \mathbf{E} = -\partial\mathbf{B}/\partial t \qquad\qquad (12)$$

$$\nabla \times \mathbf{H} = \partial\mathbf{D}/\partial t \qquad\qquad (13)$$

$$\nabla \bullet \mathbf{D} = 0 \qquad\qquad (14)$$

$$\nabla \bullet \mathbf{B} = 0. \qquad\qquad (15)$$

Here $\mathbf{E}$ represents the electric field vector of propagating light, $\mathbf{B}$ the magnetic field vector, and

$\mathbf{D} = \varepsilon\mathbf{E}$ and $\mathbf{B} = \mu\mathbf{H}$ (ε is the medium's dielectric constant, μ is its permeability).[9]

Relating these four equations to one another, the standard differential wave equations for

light's electric and magnetic fields are

$$\nabla^2\mathbf{E} = \varepsilon\mu(\partial^2\mathbf{E}/\partial t^2) \qquad\qquad (16)$$

$$\nabla^2\mathbf{H} = \varepsilon\mu(\partial^2\mathbf{H}/\partial t^2). \qquad\qquad (17)$$

Given the cylindrical geometry of a fiber, to describe light traveling through a fiber, it becomes

most convenient to express electromagnetic waves in terms of cylindrical coordinates. If the

waves, electric and magnetic, are to propagate along the z-axis of a fiber, they will take the form

$$\mathbf{E} = \mathbf{E}_0(r,\phi)e^{i(wt - \beta z)} \tag{18}$$

$$\mathbf{H} = \mathbf{H}_0(r,\phi)e^{i(wt - \beta z)}, \tag{19}$$

which are harmonic in time t and coordinate z. Here, r is the distance in the radial direction

(measured from the fiber's z-axis) and φ is the azimuthal angle about the fiber axis. Each

mode's β is determined by the boundary conditions on the electromagnetic fields at the core-

cladding interface. Plugging (18) and (19) into (16) and (17), and simplifying, the z-components

of the electric and magnetic fields satisfy

$$\partial^2 E_z/\partial r^2 + (1/r)(\partial E_z/\partial r) + (1/r^2)(\partial^2 E_z/\partial\phi^2) + q^2 E_z = 0 \tag{20}$$

$$\partial^2 H_z/\partial r^2 + (1/r)(\partial H_z/\partial r) + (1/r^2)(\partial^2 H_z/\partial\phi^2) + q^2 H_z = 0, \tag{21}$$

where $q^2 = k^2 - \beta^2$. Furthermore, the r- and φ- components of the electric and magnetic fields are

related to derivatives of the z-components of the fields by

$$E_r = -(i/q^2)(\beta\frac{\partial E_z}{\partial r} + \frac{\mu w}{r}\frac{\partial H_z}{\partial\phi}) \tag{22}$$

$$E_\phi = -(i/q^2)(\frac{\beta}{r}\frac{\partial E_z}{\partial\phi} - \mu w\frac{\partial H_z}{\partial r}) \tag{23}$$

$$H_r = (-i/q^2)(\beta\frac{\partial H_z}{\partial r} - \frac{w\varepsilon}{r}\frac{\partial E_z}{\partial\phi}) \tag{24}$$

$$H_\phi = -(i/q^2)(\frac{\beta}{r}\frac{\partial H_z}{\partial\phi} + w\varepsilon\frac{\partial E_z}{\partial r}) \tag{25}$$

Using separation of variables, the solution sets for eqns. (20) and (21) can be obtained.

Assuming that the z-component of the electric field can be written as the product of several

functions, each function only depending on a single variable, then the electric (magnetic) field

solutions take the general form

$$E_z = AF_1(r)F_2(\phi)F_3(z)F_4(t), \hspace{2cm} (26)$$

where

$$F_3(z)F_4(t) = e^{i(wt - \beta z)}, \hspace{2cm} (27)$$

since the wave is harmonic and propagates in the z-direction.[9] The circular symmetry of the

waveguides forces the electric field to have the same value when the azimuthal angle increases

by an integer multiple of 2π. Therefore, the function is periodic in the azimuthal direction, given

by

$$F_2(\phi) = e^{iv\phi}, \hspace{2cm} (28)$$

where v takes on integer values. Substituting (28), (27), and (26) into (20), then

$$\partial^2 F_1/\partial r^2 + (1/r)(\partial F_1/\partial r) + (q^2 - v^2/r^2)F_1 = 0. \hspace{1cm} (29)$$

Equation (29) is the form for a common set of differential equations whose solutions are Bessel

functions. A similar result can be derived using H_z.[9] Bessel functions dictate the nature of a

mode's electric and magnetic fields in an optical fiber. Each azimuthal parameter, v,

corresponds to a Bessel function of order v. Figures 9 and 10 contain plots of several Bessel

functions of the first kind (J_v) and Bessel functions of the second kind (K_v).

Typically, the core of a fiber is very small compared to the cladding. Therefore, the

cladding radius is assumed to be infinite (this is a valid approximation when treating fibers

whose cladding thickness is $>> \lambda$). Within the core, where $r < a$ (a = the radius of the core), the

electric and magnetic fields must remain finite. Outside the core, as $r \to \infty$, the solutions must

approach zero. To satisfy these stipulations, the solutions within the core are Bessel functions of

the first kind of order v (Figure 9) and are expressed as

$$E_z(r < a) = AJ_v(ur)e^{iv\phi}e^{i(wt - \beta z)} \qquad (30)$$

$$H_z(r < a) = BJ_v(ur)e^{iv\phi}e^{i(wt - \beta z)}, \qquad (31)$$

where A and B are constants and

$$u^2 = k_1^2 - \beta^2, \qquad (32)$$

where k_1 equals $2\pi n_1/\lambda$.
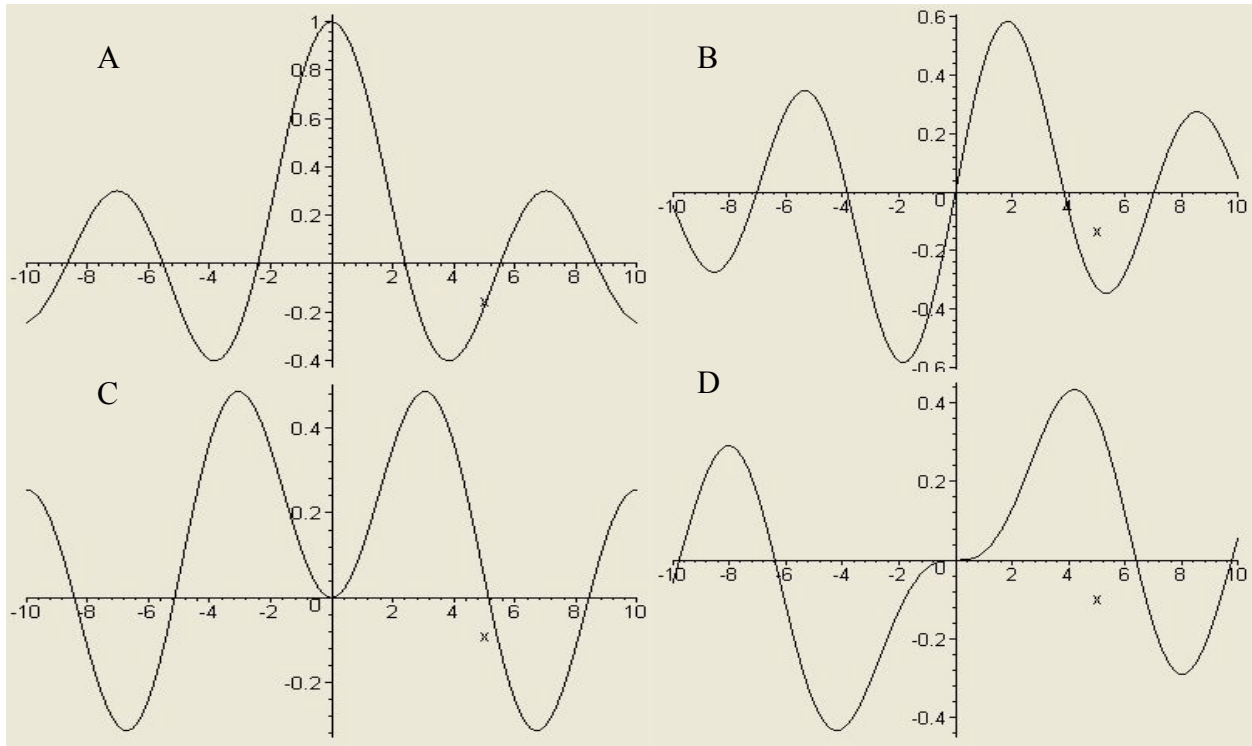
Figure 9: Some low-order Bessel Functions of the first kind. These functions can describe
the electric and magnetic field distributions within the core of an optical fiber. A) J_0. B) J_1.
C) J_2. D) J_3.

Outside the core, the solutions to the cylindrical wave equations yield modified Bessel

functions of the second kind of order v (Figure 10) and are expressed as[9]

$$E_z(r > a) = CK_v(wr)e^{iv\phi}e^{i(wt - \beta z)} \qquad (33)$$

$$H_z(r > a) = DK_v(wr)e^{iv\phi}e^{i(wt - \beta z)}, \tag{34}$$

where C and D are constants and

$$w^2 = \beta^2 - k_2^2, \tag{35}$$

where $k_2 = 2\pi n_2 / \lambda$.
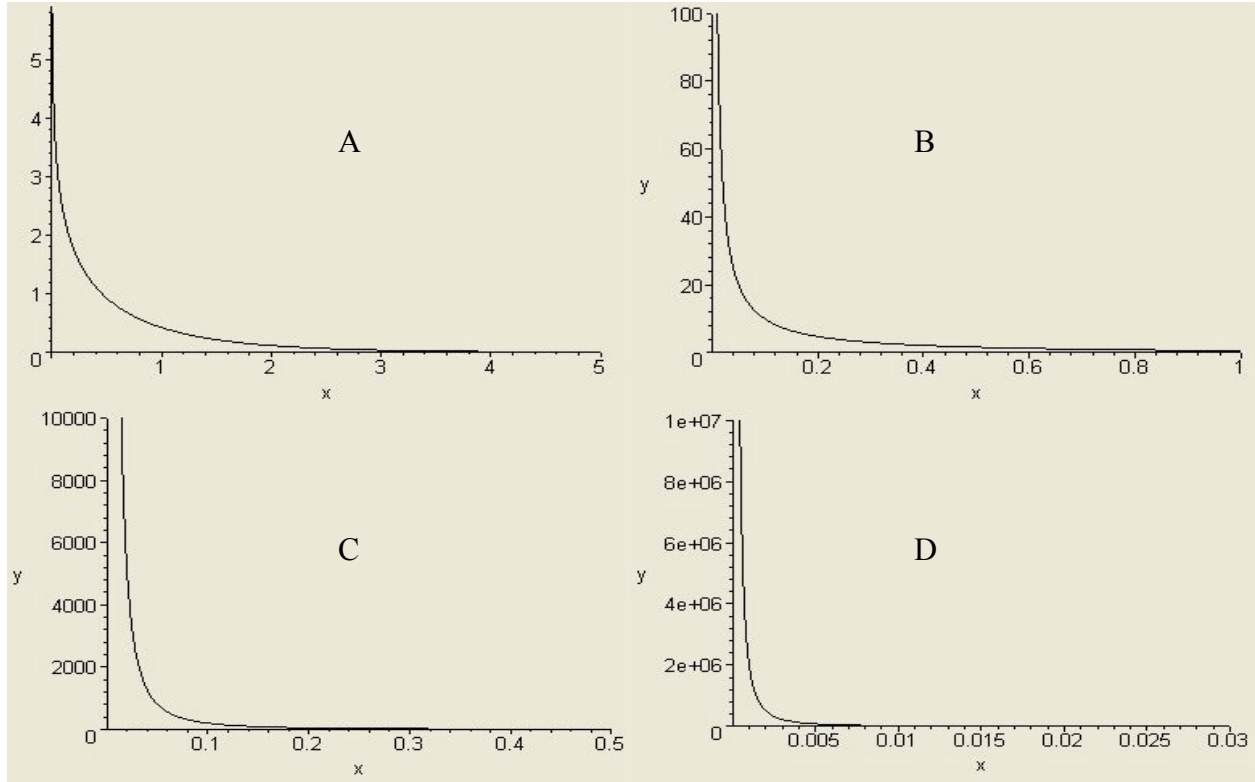
Figure 10: Some low-order Bessel Functions of the second kind. These functions can describe the electric and magnetic field distributions in the cladding of an optical fiber. A) K_0. B) K_1. C) K_2. D) K_3.

The core-cladding boundary conditions require that the tangential components of the electric field (i.e. E_z and E_ϕ) and the tangential components of the magnetic field (i.e. H_z and H_ϕ) must be continuous across the core-cladding interface. The coefficients A, B, C and D can be found by applying these conditions. Solutions for these coefficients only exist for certain, discrete values of β. Thus, the application of these boundary conditions provides a means for

finding the propagation constant of each mode as well as the number of allowed modes within

the core (one for each β).

The total number of allowed modes in a waveguide is reduced in the case that the

difference in refractive index between the core and the cladding is very small. This is a good

approximation in the experiments later discussed, where the index difference is less than 1%.

This smaller set of allowed modes is called the linearly polarized (LP) modes.

In the linearly polarized case, the application of the boundary conditions at the core-

cladding interface leads to the following transcendental equation that must be solved in order to

find the propagation constants for the modes:

$$u\mathrm{J}_{j-1}(ua)/\mathrm{J}_{j}(ua) = -w\mathrm{K}_{j-1}(wa)/\mathrm{K}_{j-1}(wa), \qquad (36)$$

where $j = v - 1$. The number of roots to eqn. (36) equals the number of allowed modes.

The number of allowed modes also depends upon the parameter

$$V = (2\pi a/\lambda)(\mathrm{n}_1{}^2 - \mathrm{n}_2{}^2)^{\frac{1}{2}}, \qquad (37)$$

often called the V-number. In general, the number of allowed modes increases as the V-number

gets larger. Thus, waveguides with large core sizes with respect to the wavelength of the light

used, or waveguides with large differences in refractive index between the core and cladding,

tend to support more modes.

If more than one mode is allowed to propagate, the waveguide is called multi-mode.

However, if the physical characteristics of the waveguide and the wavelength of the incident

light permit, the waveguide will only support one mode. In that case, the waveguide is called

single-mode. For single-mode operation, there must be only one root to eqn. (36) and V must be

≤ 2.405.

When constructing a nonlinear capillary limiter, single-mode operation provides a number of benefits. Single-mode waveguides tend to have very small core diameters. Within such a small geometry, light focused into the core remains extremely intense, inducing a nonlinear response against very low input energies. Also, most commercial fiber systems utilize single-mode optical fibers. Thus, single-mode limiters are more easily integrated into these systems.

c) Computerized Mode Finding

For analysis of waveguides discussed in this project, a MathCAD computer program was used to find the number of roots to eqn. (36). The program plots each side of the transcendental eqn. (36). It also computes the V-number associated with input fiber characteristics. This information indicates the number of modes a fiber will support and each mode's corresponding effective refractive index.

Consider a waveguide having the characteristics listed in Table 1.

Table 1

Core Radius	1.5 μm
Operating Wavelength	532 nm
Core Index (n_1)	1.486
Cladding Index (n_2)	1.482

In Figure 11, the MathCAD program plots each side of eqn. (36) using the parameters from Table 1. The program also returns the V-number associated with the given characteristics:

$$V = 1.93$$

In Figure 11, the solid curve represents the plot of the left side of eqn. (36) versus n_{eff}, where n_{eff} ranges between n_1 and n_2. The dotted curve is the plot of the right side of eqn. (36) versus the same range. Because the two lines only cross once (equivalent: eqn. (36) has only one root) and

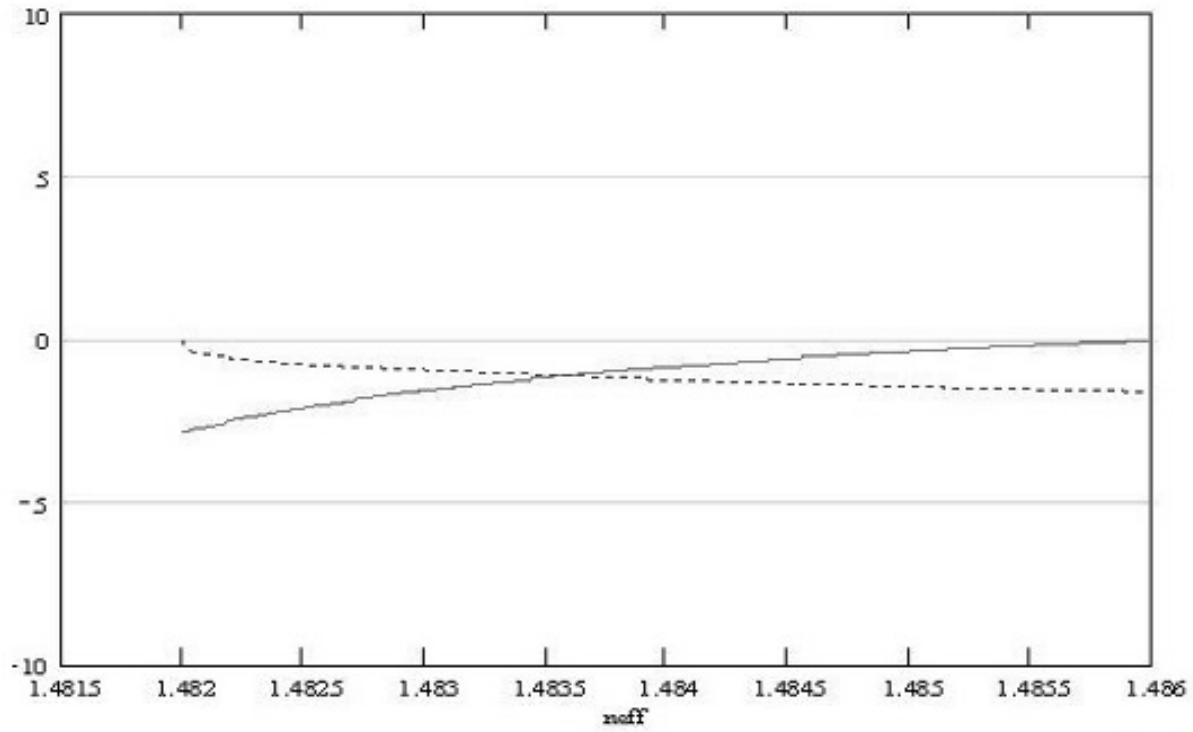**Figure 11:** The plot of the left and right sides of eqn. (36). The graph indicates that, for the parameters given in Table 1, eqn. (36) exhibits only one root. The solid curve represents the left side of eqn. (36), the dotted curve is the right side of eqn. (36).

since the V-parameter remains less than 2.405, the fiber allows only one mode to propagate. As the graph indicates, this lone mode displays an effective index ~ 1.4837.

3. The Multi-Mode Limiting Apparatus

Designing a limiting apparatus for experimental purposes proved a difficult and time

consuming process. The device had to be easily reproducible, its reproductions had to yield

consistent results, it had to give easy access for external optics and it had to be inexpensive.

Through its evolution, the design took many forms, but in the end, the simplest device proved

best.

The main component of the
limiter design is, as mentioned
before, the capillary tube.
Fabricated by stretching fused silica,
the capillary material is purchased
by the meter. The capillaries used in
the design exhibit internal diameters

Figure 12: A graphic depiction of the optical waveguide limiter design devised for this project.

(ID) ranging from ~3 to ~200 microns. In all cases, capillary outer diameters (OD) were much

larger than the core inner diameters. After cleaving the bulk material into 1.8 cm segments (1.8

cm is the smallest segment the cleaving machine can produce), the capillaries were filled with

solutions (linear or nonlinear) by capillary action. Given the viscosity of the tested solutions, the

capillaries could take quite a while to fill. To illustrate, 10-micron (ID) capillaries typically

filled within two hours. The more slender 3-micron (ID) capillaries sometimes required 24 hours

to completely fill.   This filling method proved quite adequate, although on infrequent occasions

bubbles formed within the capillaries and rendered them useless.

The construction of the apparatus is quite simple. Two thin optical flats (microscope

slide covers) stand on end, parallel to one another (see Figure 12). The flats are glued to a stable

platform in this conformation. Held in place between the parallel flats, running perpendicular to the face of each flat, a capillary is suspended. Each end of the capillary waveguide butts against one of the optical flats.

During experiments, laser light (focused by a microscope objective) funnels through the input optical flat into the core of the suspended waveguide. Propagating through the nonlinear core, the input light stimulates a limiting response. At the output of the waveguide, a second objective re-collimates the light into a coherent beam for observation.

4. The Investigated Nonlinear Material

A. Silicon Naphthalocyanine

Nonlinear capillary waveguides discussed in this report incorporate the nonlinear substance called bis[tri-(n-hexyl)siloxy] silicon naphthalocyanine (SiNc).[4] SiNc, a solid at room temperature, acts as a reverse-saturable absorber when irradiated with 532 nm-wavelength light. SiNc's properties actually make it an RSA molecule over a broad portion of the visible spectrum, and it displays limiting characteristics against wavelengths from ~ 400 nm to ~ 600 nm.[4] Thus, SiNc would be an adequate nonlinear molecule for optical limiting applications that require limiting in the visible spectrum. The experiments presented in this report irradiated SiNc with only 532 nm-wavelength (green) light.

In actuality, SiNc's molecular energy scheme cannot be fully described by a three-level model (like the schematic presented in Figure 3). Figure 13 shows SiNc's actual molecular

Figure 13: SiNc's energy schematic. SiNc displays a nonlinear reverse-saturable character because σ_s and σ_t are $> \sigma_g$. SiNc's ability to limit very short light pulses is affected by the lifetime of the s_1-to-t_1 decay. For incident pulses shorter than 4.5 ns, SiNc's absorption ability decreases (the s_1-to-s_2 transition becomes more likely than the t_1-to-t_2).
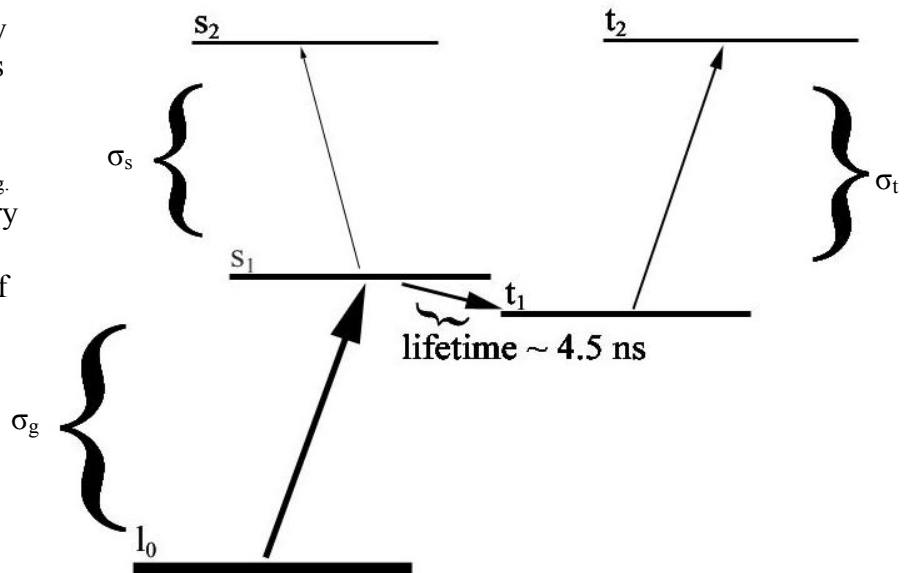
energy scheme, which includes five levels. If no outside energy source stimulates a SiNc molecule, it remains in a low energy state (its ground state, l_0, holds the vast majority of the

molecule's associated electrons). Under photon irradiation, electrons in the ground state interact with bombarding photons and transit to the first excited singlet state (s_1). From s_1, electrons can take a number of pathways: if the fluence of an incident pulse of photons is insufficient to stimulate further excitations, the excited electrons will de-excite back down to l_0 (perhaps via state t_1); if the incident pulse fluence is large enough, electrons can excite again to the second excited singlet state (s_2); or, they can drop to the first excited triplet state (t_1) and then excite to the second excited triplet state (t_2). In the case of an intense incident pulse, observations have established the fraction of electrons that transit from s_1 to s_2 versus the fraction of electrons that transit from s_1 to t_1 and then on to t_2.[4] For intense pulses longer than the 4.5 ns lifetime of the s_1-to-t_1 transition, experiments have shown that ~ 75% of electrons in s_1 remain in s_1 to transit to s_2, while 25% of the electrons in s_1 decay to t_1 and become vulnerable to further excitation to t_2.

It is the possibility of the t_1-to-t_2 and s_1–to-s_2 transitions that make SiNc a reverse-saturable absorber. These transitions exhibit absorption cross-sections (σ_t and σ_s, respectively) much greater than the ground state absorption cross-section (σ_g). In SiNc, uncertain measurements (measured using an 8 ns pulse) place σ_t somewhere in the range of 46 x 10^{-18} cm^2 to 115 x 10^{-18} cm^2, while σ_s is more exactly measured at ~ 33.4 x 10^{-18} cm^2.[4] σ_g takes the relatively low value of 2.3 x 10^{-18} cm^2 (no matter the incident pulse length). That is, an electron transition from t_1 to t_2 is about 50 times more likely, and an electron transition from s_1 to s_2 is about 14 times more likely, to absorb a photon's energy than an electron transition from l_0 to s_1. Once incident light intensity becomes high enough to significantly populate state s_1 and force transitions to s_2 and t_2, SiNc's absorbing ability greatly increases.

B. The Reduced Three-Level Model

For the sake of ease in building a computer model of SiNc's nonlinear response to light, the molecule's complex energy level structure is reduced to an approximately equivalent three-level model (see Figure 14). This approximation proves accurate for the purposes of this project and makes computer simulations much more computationally efficient. The three-level model condenses the original states s_1 and t_1 into one state (l_1), and it condenses states s_2 and t_2 into a separate higher state (l_2).

In modeling the results of this project, an approximate value for the effective excited absorption cross-section (σ_{eff}) can easily be calculated (σ_g remains 2.3 x 10^{-18} cm^2). Using the relationship

$$\sigma_{eff} = (\sigma_s f_s + \sigma_t f_t), \tag{38}$$

where f_s (= 0.75, measured using an 8 ns, 532 nm-wavelength light pulse) represents the fraction of electrons making the s_1–to-s_2 excited transition and f_t (= 0.25) represents the fraction of electrons making the t_1–to-t_2 transition (see Figure 13).[4] The pulses used for investigation in this project lasted either ~ 7 ns or ~ 5 ns. Because the f_s and f_t were measured using an 8 ns pulse, another factor must be taken into account when calculating σ_{eff}. In the case of the 7 ns pulse, the result harvested from eqn. (38) must be multiplied by (7/8). For the 5 ns pulse, the result must be multiplied by (5/8). In the end,

Figure 14: SiNc's reduced three-level schematic.

$$31.9 \text{ x } 10^{-18} \text{ cm}^2 < \sigma_{\text{eff}} < 47.1 \text{ x } 10^{-18} \text{ cm}^2 \qquad\qquad 7 \text{ ns pulse}$$

or

$$22.8 \text{ x } 10^{-18} \text{ cm}^2 < \sigma_{\text{eff}} < 33.6 \text{ x } 10^{-18} \text{ cm}^2. \qquad\qquad 5 \text{ ns pulse}$$

For the reduced three-level model, the ratio $\sigma_{\text{eff}}/\sigma_g$ determines SiNc's nonlinear ability.

Beyond a certain threshold of incident fluence, both the three- and five-level models become inaccurate. If the incident pulse is intense enough, it will fully saturate SiNc's excited levels. In this case, once the upper levels totally saturate, SiNc will begin to act like a linear absorber again because electrons will only be able to transit between the molecule's upper levels (there will be no net de-excitations to l_0). Thus, the ratio $\sigma_{\text{eff}}/\sigma_g$ becomes irrelevant, and only σ_{eff} contributes to the molecule's absorptive coefficient.

Previous experiments conducted to test SiNc's limiting ability have shown that, in a free-space environment (not within the core of an optical waveguide), SiNc's threshold fluence, called the saturation fluence, can be determined using the relationship[4]

$$F_{\text{sat}} = \frac{h\nu}{\sigma_g \Phi_t}. \qquad\qquad (39)$$

Here, F_{sat} stands for the saturation fluence, h is Planck's constant, ν is the frequency of incident light, σ_g is the ground-state absorption cross section, and Φ_t is the triplet excited state's quantum yield. Φ_t is an index that indicates the how easily the first triplet excited state is populated—it relates directly to the fraction of electrons that populate level t_1. Using (39), against 532 nm-wavelength light, SiNc's saturation fluence is $\sim .464 \text{ J/cm}^2$. This result is valid for a limiting response provoked in a free-space environment and can be used for comparison to saturation fluences achievable within nonlinear optical waveguide geometries.

SiNc is also an excellent limiter in terms of its fast response time. In previous experiments, SiNc successfully limited 8 ns laser pulses (532 nm wavelength).[4] SiNc can

certainly limit even shorter pulses (this project observed a limiting response against 4.9 ns pulses of 532 nm light). Because the lifetime of SiNc's first excited state is long (about 5 ns[4]), it is necessary to treat irradiating light pulses in terms of fluence [energy/area] rather than in terms of intensity [energy/(area*time)]. This is because the absorption experienced by each part of the pulse depends on the total amount of energy already absorbed by the material from previous parts of the same pulse. The increase in absorption is a cumulative (or integrated) effect. For the rest of this report, the energy associated with a pulse will be given in terms of fluence, which indicates the amount of energy an entire light pulse delivers per unit area.

5. The Light Sources

Two different frequency-doubled, Q-switched Nd:YAG lasers were used to investigate nonlinear SiNc waveguides. The laser used at the Naval Research Laboratory (Washington, D.C.) creates ~7 ns pulses (full-width-half-max), while the laser used at the US Naval Academy creates ~ 4.9 ns pulses (full-width-half-max). Both lasers operate with a pulse repetition frequency of 10 Hz. Both lasers produce 532 nm-wavelength light. The energy-per-pulse output of each laser can be varied.

Both lasers create pulses whose temporal energy distributions are nearly Gaussian in space and time. This simple distribution provides for ease in modeling the interaction of a pulse with nonlinear material (see Figure 15).
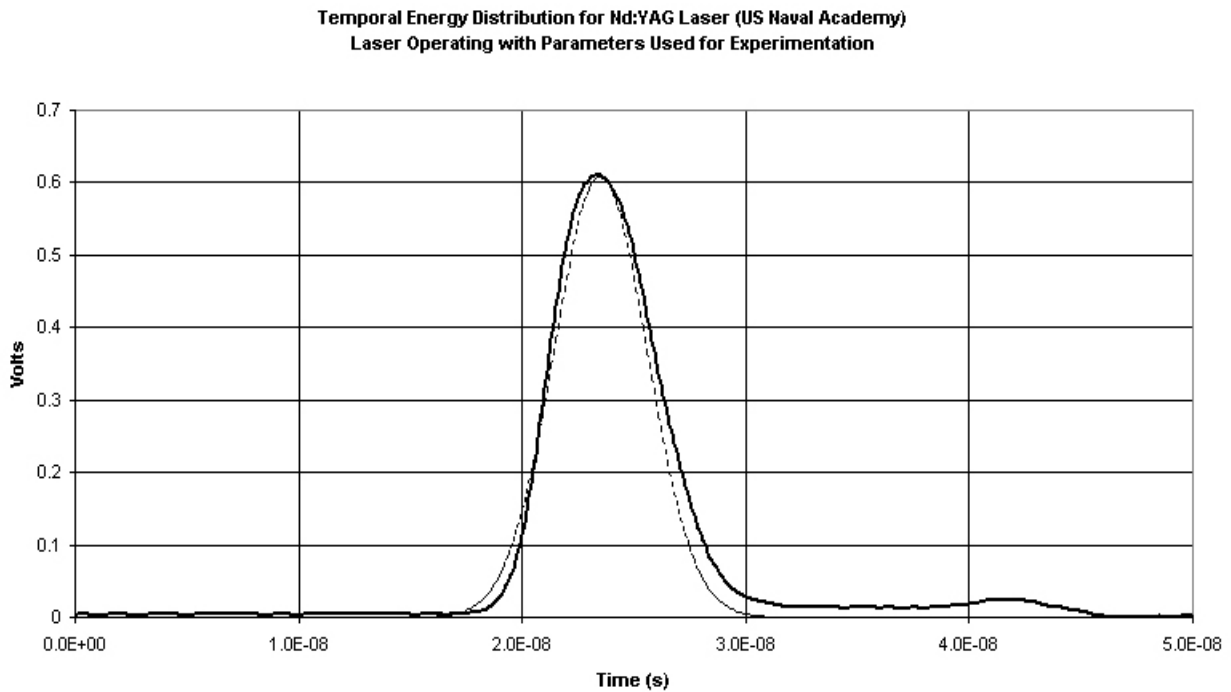
Figure 15: Temporal energy distribution of the Nd:YAG laser used at the US Naval Academy. The thick line represents the actual distribution. The dotted line represents a perfect Gaussian distribution. The pulse lasts ~ 5 ns (at full-width-half-max).

6. Experimental Setup

The experimental setup used to test nonlinear waveguides facilitated ease in switching

test samples and provided means to measure waveguides' transmission characteristics.

Experimental setups at the Naval Research Laboratory and the US Naval Academy were

identical. This section describes the setup, optic-by-optic (see Figure 16).

Figure 16: The experimental setup (bird's eye view). The green lines indicate the beam path. The letters denote each optical element.
A. - Laser; B. and C. - 5% reflecting prisms; D. - Fully reflecting mirror; E. - Spatial filter; F. - Lens; G. - Variable diameter aperture; H. - Variable waveplate retarder; I. - Beam-splitter; J. and K. - Energy sensors; L. and N. - Microscope objectives; M. - Waveguide sample.
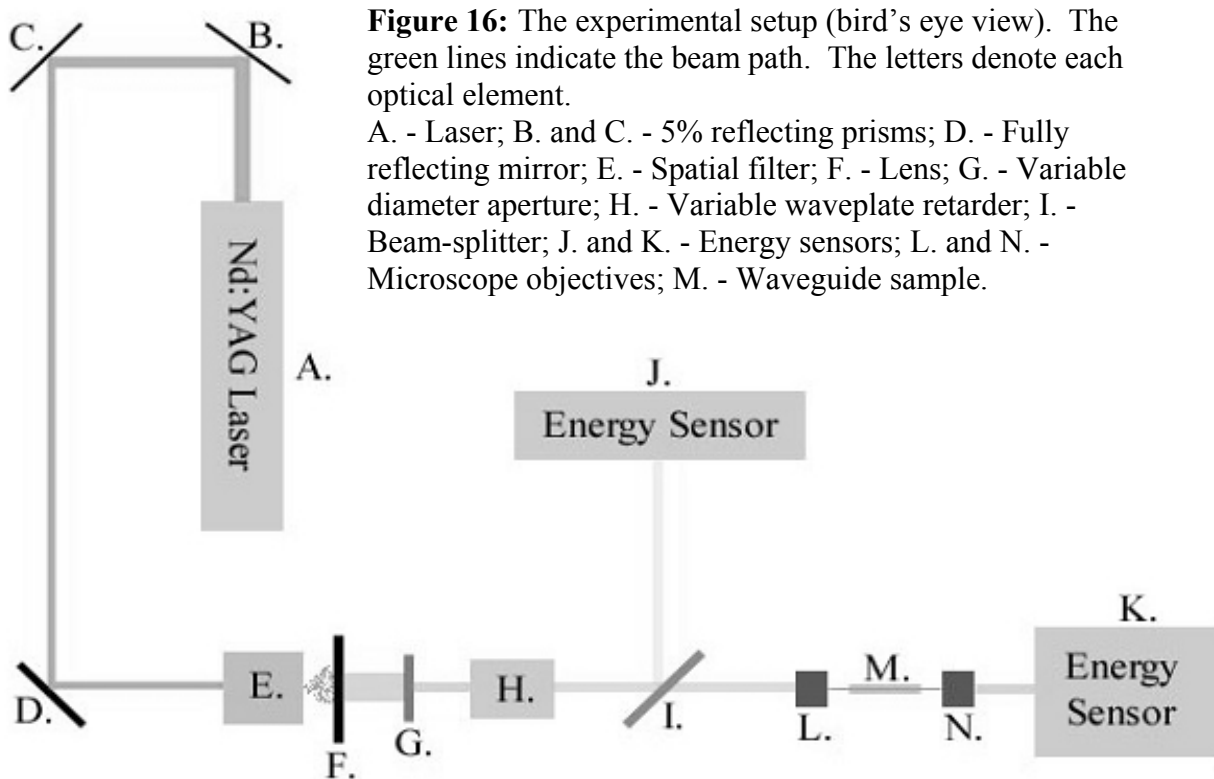
A pulse leaving the source laser first reflects off of two partially reflecting prisms (B and

C in Figure 16). These prisms, each reflecting 5% of the propagating pulse, reduce the energy

associated with the pulse to 0.25% of its original strength. This reduction ensures that the pulse

will not damage the waveguide sample or other optics in the setup. From the prisms, the pulse

hits and reflects off of a fully reflecting mirror (D), which aims the beam towards the next series

of optics.

Next, the pulse travels into a spatial filter (E). The filter ensures the spatial energy

distribution of the pulse is a nearly Gaussian profile. It consists of a microscope objective

followed by a 5 μm pinhole. The microscope objective focuses the incident pulse. The pinhole,

placed at the focal point of the objective, only allows an approximately Gaussian energy profile

to propagate through it. Thus, as the pulse focuses through the pinhole, the pinhole filters out

any noise not contributing to a Gaussian energy distribution. On the output side, the pinhole acts

like a point source, emitting the pulse in a spherically symmetric spread. A lens (F) collimates

the light emitted from the pinhole.

Upon leaving the lens, the pulse travels through a variable-diameter aperture (G). The

aperture shrinks the transverse diameter of the propagating pulse to the optimal size; obtaining

maximum coupling efficiency into the target waveguide requires that the input beam have the

proper diameter. The input beam's proper diameter can be approximately determined from the

characteristics of the target waveguide and the from the characteristics of the objective used to

focus the beam into the target waveguide by using the relationship

$$d_0 = (4\lambda f)/(\pi d_1), \tag{40}$$

where d_0 is the diameter required of the input pulse (the diameter of the target waveguide's core),

λ is the wavelength of incident light, f is the focal length of the objective employed and d_1 is the

diameter of the target waveguide's core. This relationship assumes that the input beam has a

Gaussian spatial profile.[7] The aperture is set to have a diameter $= d_0$.

From the aperture, the pulse enters a variable waveplate retarder setup (H). Although

Figure 16 represents the waveplate retarder setup as a single element, the instrument actually

consists of three optics: firstly, a polarizing prism; secondly, the variable waveplate itself; lastly,

another perpendicularly oriented polarizing cube. The variable waveplate allows the user to vary

the intensity of the propagating pulse. Light emerging from the laser is linearly polarized, but not perfectly. The first polarizing prism is oriented so that it transmits essentially all of the light. The prism cleans up the incident pulse so that, by the time the pulse reaches the variable waveplate, it is perfectly polarized. The waveplate, having some voltage applied across it, rotates the polarization of the pulse away from the original polarization. From the waveplate, the pulse continues on to the second, perpendicularly oriented polarizing prism. This prism only allows transmission of the portion of the pulse that shares its (the prism's) polarization. Depending upon the voltage applied to the waveplate, and therefore on how much the waveplate rotates the polarization of the pulse, the second polarizing cube only transmits a fraction of the incident energy. The amount that the waveplate alters the polarization of the pulse is adjusted by an electronic control circuit. Thus, the fluence of the pulse emerging from the second prism can be continuously adjusted by turning a knob on the control circuit.

The attenuated pulse then interacts with a beam-splitter (I). The beam-splitter allows approximately 92% of the pulse to transmit, but reflects 8% at a skew angle. The reflected 8% propagates to an energy sensor (J). This energy sensor measures the energy associated with the reflected portion of the pulse. By considering the efficiency of the beam-splitter, the energy associated with the transmitted 92% (the portion of the pulse that actually transmits to the waveguide's entrance) can be determined.

The transmitted pulse continues on to an objective (L). This objective—experiments used a 10X microscope objective—focuses the input pulse. At the objective's focal point, the pulse couples (at least partially) into the core of the target waveguide (M). A particular waveguide's coupling efficiency can be empirically determined for use in data analysis.

At the target waveguide's output side, the emitted light is collected by another objective (N). Usually a 50X, 20X or 10X objective, this optic re-collimates the emitted light into a coherent pulse. The pulse continues to an output energy sensor (K). By comparing the waveguide's output energy to its input energy and factoring in its coupling efficiency, the waveguide's nonlinear limiting capability can be deduced.

7. Methodology

After the waveguide is constructed, it is placed into the source laser's beam path, between the input and output objectives. The input objective is then aligned to focus light pulses into the waveguide. This alignment process can take hours—focusing light into a waveguide's core (sometimes no more that 2 microns in diameter) can prove a daunting task. After achieving maximum coupling efficiency into the waveguide's core, the output objective is aligned to project light to an output energy sensor.

Data collection now proceeds. The laser source fires pulses into the waveguide, beginning with input energies no more than about 1 or 2 pJ per pulse. The energy per pulse is slowly increased to a maximum. Based upon the characteristics of the waveguide being tested, this maximum energy will vary. For example, input energy per pulse for 10 μm ID waveguides reaches a maximum of about 1 μJ; energy per pulse for 5 μm waveguides reaches a maximum at 250 nJ; and maximum energy per pulse for 2 μm waveguides is 100 nJ. Higher energies than these threaten to damage samples. The energy sensors (see Figure 16) collect the energies entering and exiting a sample for each pulse. These data are then sent to a computer and inserted in a spreadsheet. For a given data run, thousands of data points are collected. The entire process, start to stop, can take up to fourteen hours.

Besides testing for transmission characteristics, the energy distributions at the waveguide's output end are observed for different input energies. A digital camera utilizing a 1.4 mega pixel CCD array (Charge Coupled Device) takes snapshots of the waveguide's output side. These images are sent to a computer for collection. Specialized software is used to measure the percentage of total light energy each pixel receives. In this way, the software builds

an energy distribution map of the received pulse. The energy distribution images (like the one in

Figure 8) help determine the modal structure propagating through the waveguide's core.

8. Computer Modeling of SiNc

The Fortran computer program (see Appendix A) used to simulate SiNc's nonlinear response operates on the principles explained above. Researchers at the Naval Research Laboratory wrote the program to model the limiting responses of various RSA molecules. The program does not account for the physical situation created within a nonlinear waveguide. It was devised to model free-space optical limiters, for which there are virtually no boundary conditions placed on the electromagnetic distribution of propagating light. However, because most of the waveguide optical limiters tested in this project are highly multi-mode, this program is expected to simulate their limiting responses well.

The program simulates the firing of light pulses, each pulse being more energetic than its predecessor, into the core of a nonlinear waveguide. By accounting for the absorptive ability of the nonlinear core, the program calculates the amount of energy-per-pulse the nonlinear waveguide should transmit for each incident pulse. The program plots two columns of simulated data—one column for energy in (per pulse), one column for energy out (per pulse).

To create a simulated plot, the program first needs to know the specific parameters of the optical limiter being simulated, such as: incident wavelength, SiNc's σ_g, the waveguide's core diameter (R_0), SiNc's σ_e, the concentration of SiNc molecules in solution (C_0), the length of the waveguide (L_0), the full-width-half-max pulsewidth (Tfwhm) of the incident light pulses, and the initial energy-per-pulse (E_0).

The program first calculates the waveguide's linear transmission by assuming that, initially, all of the molecules in solution are unexcited. To do this, it takes SiNc's σ_g (the ground-state absorption cross section) and the molar concentration of the solution (C_0) and

combines them in eqn. (5). When all the molecules are unexcited, the solution's overall

absorption coefficient, α, is

$$\alpha = \alpha_g = \sigma_g C_0 N_A \left(\frac{1\,L}{1000\,mL}\right), \qquad (41)$$

where C_0 is the molar concentration of the SiNc solution and N_A is Avogadro's Number. The

program considers α and the waveguide's length (L_0) to calculate the fractional linear

transmission (T_{linear}) the waveguide should display:

$$T_{linear} = e^{-\alpha L_0} \qquad (42)$$

Assuming that a simulated incident pulse has an initial energy E_0, then the maximum transmitted

energy is given by (T_{linear})(E_0).

In order to account for the nonlinear core's absorptive ability (over and above the linear

ground-state absorption), the simulation begins by building a mathematical representation of the

core as a cylinder. This cylinder (defined using a cylindrical coordinates system) has some

radius and some length (i.e. the radius and length of the core being simulated). Thus, every point

in the core can be represented by a set of coordinates, (r, φ, z). However, because the simulated

pulse exhibits a Gaussian energy distribution in both space and time—the pulse is azimuthally

symmetric—it is unnecessary to consider the φ-coordinate of the core for these simulations.

Next, the program builds a simulated input pulse. For the temporal width of the pulse,

the program takes the full-width-half-max (FWHM) pulsewidth entered earlier (for example, the

laser at Naval Research Laboratory creates FWHM pulses lasting 7 ns). The transverse (spatial)

width of the pulse is assigned the same width as the waveguide's core diameter. As the program

iterates forward in time, this pulse will gradually propagate through the core of the simulated

waveguide.

The program now assigns an initial time from which to start the simulation. It begins by determining the length of the 1/e pulsewidth from the FWHM pulsewidth (the 1/e pulsewidth is another convention used to discuss the temporal length of a pulse)

$$Tp = \frac{Tfwhm}{2\sqrt{\ln^{-1}(2)}} ,$$ (43)

where Tp is half the pulse's 1/e pulsewidth. Using Tp, the program calculates T_0, the initial time

$$T_0 = -2.5Tp.$$ (44)

Setting T_0 to this value, the simulation begins well before the simulated pulse comes into contact with the simulated waveguide's core.

As an example of how the program performs transmission calculations, consider the pulse interacting with the waveguide at some time, t. At this instant, the program simulates the pulse as extending through the core along the z-axis, such that each point in the core is interacting with a different number of photons (because the program assigns the pulse a Gaussian energy distribution, it introduces different numbers of photons to different points in the core).

Because a nonlinear material's absorptive ability depends upon the density of photons (energy) present, then each portion of the core will absorb a different fraction of photons. The more photons present in a differential volume of the core, the higher the fraction of photons that volume can absorb. The program determines the number of photons, G, present in a differential volume in the core using

$$G = \frac{I(r,z,t)}{h\nu} dt ,$$ (45)

where $I(r,z,t)$ is the intensity of the pulse in that differential volume at the instant being considered, and dt is the amount of simulated time (in which the pulse propagates) before the

program again considers the photon density at this particular point. G is the number of photons that pass through the differential volume during time dt.

Using each particular volume's absorptive coefficient (see eqn. (5)), the program then calculates the fraction of photons each differential volume in the core absorbs. As a particular volume in the core absorbs photons, more of its molecules shift to the excited state. Thus, after time t, a particular volume of the core may have a higher excited-state density. For a particular volume, the program calculates the new density for the ground and excited states, using

$$G_1 = M_0 (\sigma_g)(G), \tag{46}$$

where M_0 is the previous concentration of molecules in the ground state (at that particular volume in the core). G_1 is the number of molecules which enter the excited state during time dt (in that particular volume). Thus, the new ground-state population for this differential volume (to be used in subsequent calculations) is given by

$$N_0 = M_0 - G_1, \tag{47}$$

where N_0 is the new ground-state density. And, the new excited-state density (for this volume), is given by

$$N_1 = M_1 + G_1, \tag{48}$$

where N_1 is the excited state's new density after time dt, M_1 is the excited state's density at the beginning of time dt, and G_1 is given above.

Thus, the new absorptive coefficient (for this particular volume) becomes

$$\alpha_{(r,z,t)} = \sigma_g (N_0) + \sigma_e (N_1), \tag{49}$$

which is identical to eqn. (7). The program uses the new α to determine the number of photons that the volume will absorb when the next part of the pulse arrives some small time later.

The program sums the absorptive effect calculated for all the differential volumes in the core (r,z) and all times (t) in order to find the net amount of energy the core absorbs from the incident pulse while it propagates within the waveguide. For each pulse, then, the transmission (T) is defined to be

$$T = \frac{\text{Energy Out}}{\text{Energy In}}.$$ (50)

And, relative transmission is defined to be

$$T_{rel} = \frac{T}{T_{linear}},$$ (51)

where T_{linear} is defined in eqn. (42).

9. Multi-Mode Waveguide Limiter Results

Presented below are the data taken from a number of waveguides. The data are displayed graphically and indicate the transmission characteristics of each tested waveguide. Although linear data are not presented here, all nonlinear waveguides were compared to linear waveguides having the same characteristics. Nonlinear waveguides were filled with solutions of SiNc dissolved in Dioctyl Phthalate (DOP). DOP is an optically inert substance whose index of refraction ($n_D \sim 1.485$) is higher than that of the silica ($n_{532} \sim 1.462$) capillaries used to make the waveguides. Data presented were taken from waveguides with inner diameters ranging from 3.2 μm to 200 μm. Analyses of the data are presented in the subsequent section.

A. 200 μm (ID) Waveguide

Figure 17 portrays the transmission characteristics of a 200 μm ID nonlinear waveguide. In this case, the waveguide's core was a solution of SiNc concentrated in DOP at 4.23×10^{-5} mol/L. The waveguides' length was 10 cm. The nonlinear waveguide, therefore, created a linear transmission of 56%. Input pulses were 7 ns (FWHM).

These data, having been taken before the invention of the device outlined in Section 3, were procured using another, similar device. This older device also incorporated a capillary waveguide, but rather than funneling light into the waveguide through an optical flat, a commercial multi-mode fiber optic (core diameter = 100 μm) was inserted into the end of the waveguide to introduce the incident pulses to the limiting core. On the output end, a second fiber optic carried the limited pulses to the output energy sensor.

Figure 17: The relative transmission plot for the 200 μm nonlinear waveguide. The black dots represent the data, the solid line represents the simulation of the data.
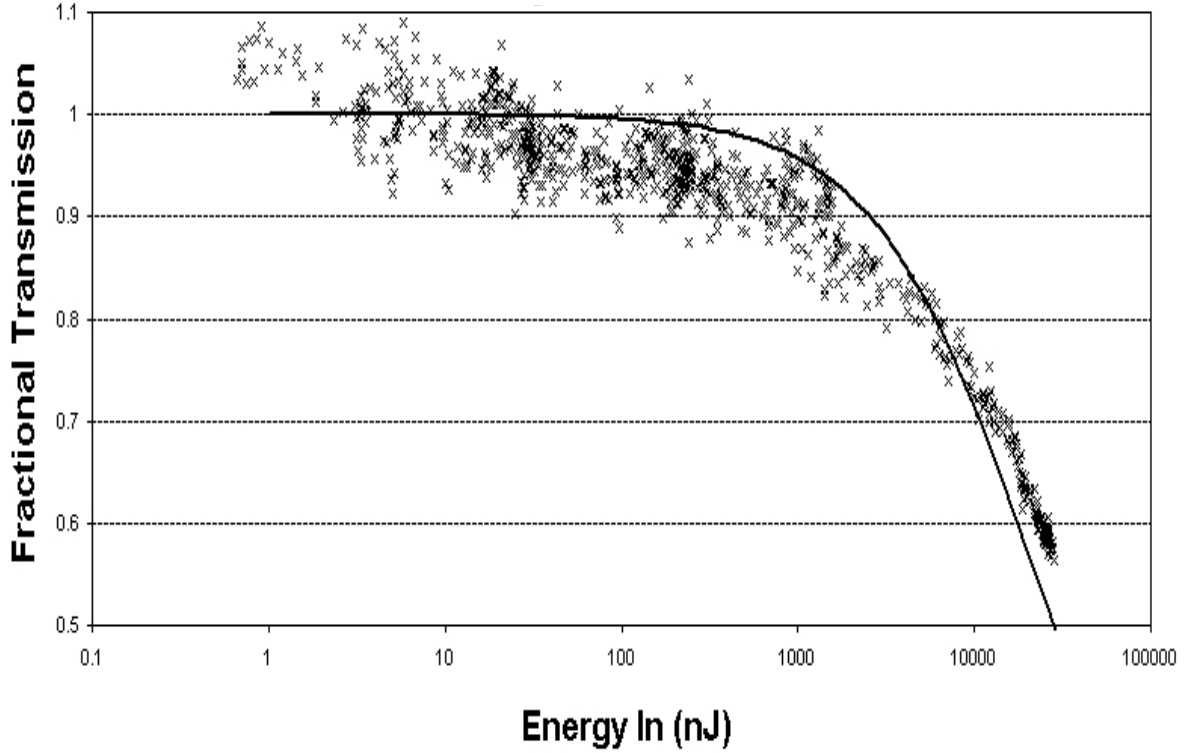
B. 75 μm (ID) Waveguide

The data presented in Figure 18 were taken from a 75 μm ID nonlinear waveguide incorporated into the same type of device used to take the 200 μm waveguide data. In this case, the concentration of SiNc in DOP was 5.81×10^{-4} (mol/L). The waveguide was 1.2 cm long. This yielded a $T_{linear} = 39\%$. The input fiber, which funneled light into the waveguide's nonlinear core, had a core diameter = 50 μm. Input pulses were 7 ns (FWHM).

Figure 18: The relative transmission plot for a 75 μm nonlinear waveguide. Gray dots are the data, the dotted line is a simulation (effective core diameter = 75 μm) and the thick line is a second simulation (effective core diameter = 35 μm).
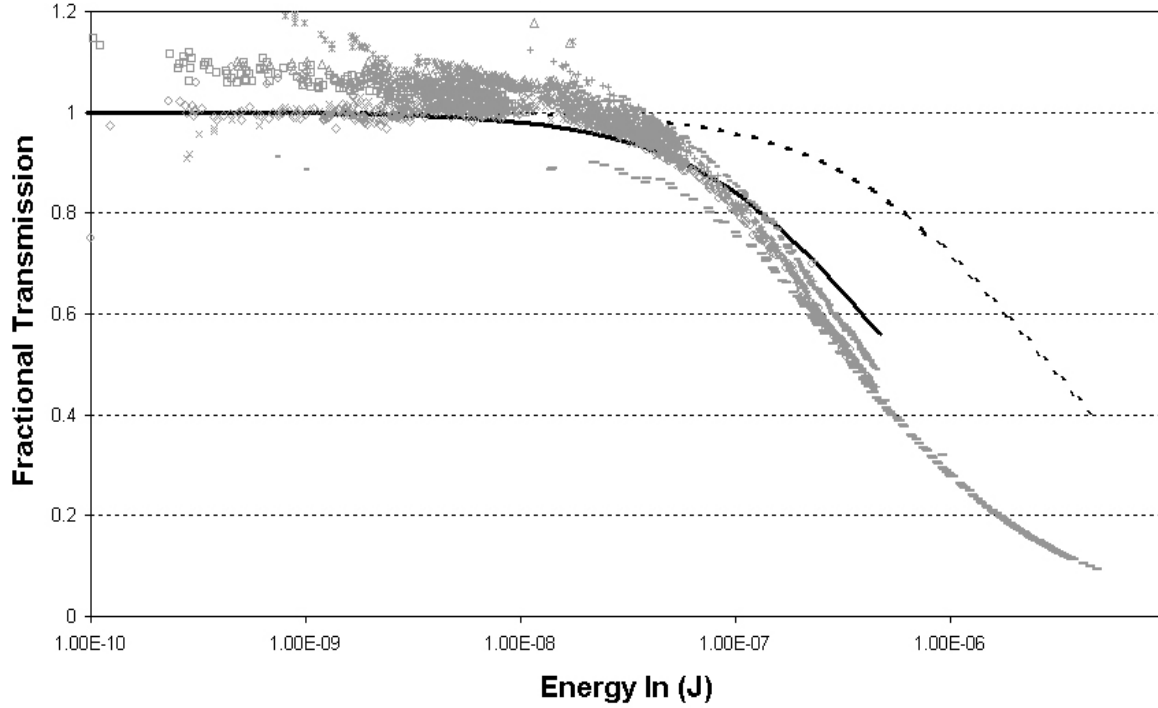
C. 10 μm (ID) Waveguide

The data presented in Figure 19 were taken from a 10 μm ID nonlinear waveguide incorporated into the device explained in Section 3. In solution, the SiNc was concentrated to 3.25×10^{-4} mol/L and the waveguide was 1.8 cm long, yielding a T_{linear} of 45% for this optical limiter. Light was focused in through the entrance optical flat using a 10X objective. The device was adjusted to yield maximum coupling efficiency into the waveguide. Input pulses were 7 ns (FWHM).

Figure 19: The relative transmission plot for a 10 μm nonlinear waveguide. Gray dots are the data, the slender line is a simulation (effective core diameter = 10 μm) and the thick dotted line is a second simulation (effective core diameter = 3.4 μm).

D. 6.3 μm (ID) Waveguide

The data presented in Figure 20 were taken from a 6.3 μm ID nonlinear waveguide using the device explained in Section 3. Input pulses were 5 ns (FWHM). In solution, the SiNc was concentrated to 3.25×10^{-4} mol/L and the waveguide was 1.8 cm long, which yielded a T_{linear} of 45% for this optical limiter. Light was focused in through the entrance optical flat using a 10X objective. The device was adjusted to yield maximum coupling efficiency into the waveguide.
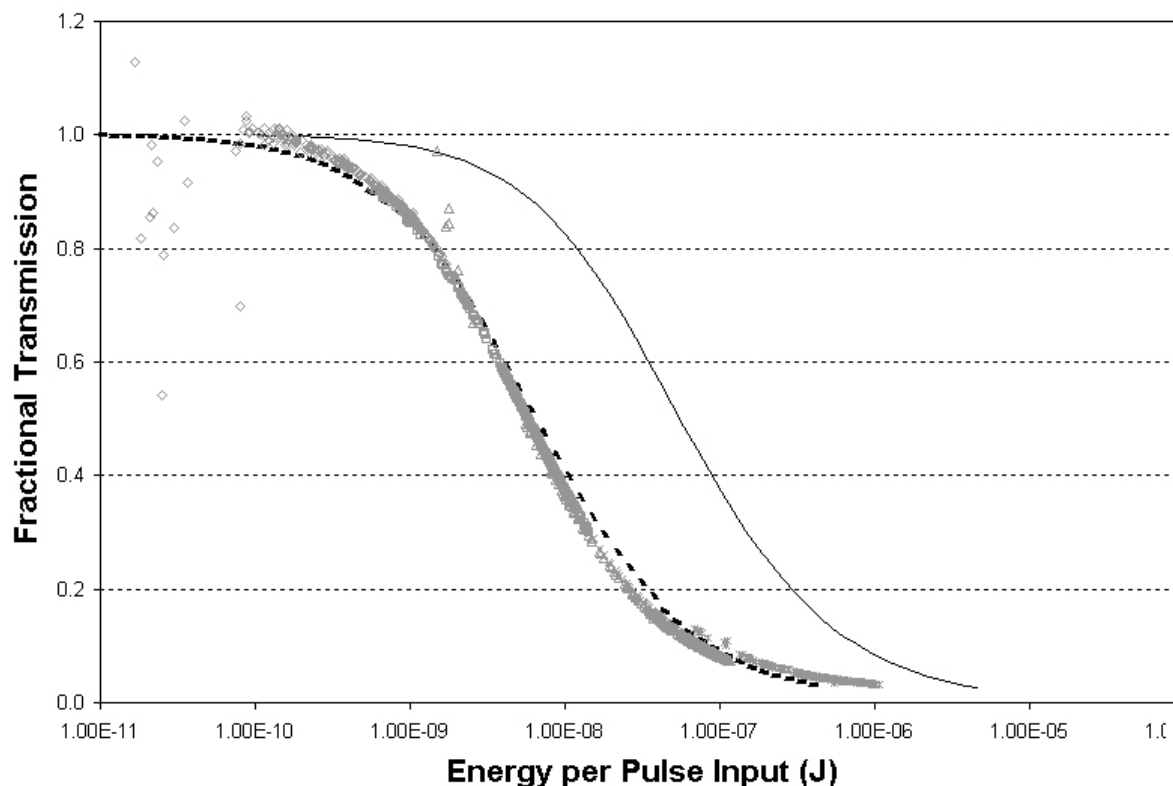
Figure 20: The relative transmission plot for a 6.3 μm nonlinear waveguide. Gray dots are the data, the opaque line is a simulation (effective core diameter = 6.3 μm) and the dotted line is a second simulation (effective core diameter = 3.4 μm).

E. 3.2 μm (ID) Waveguide

The data presented in Figure 21 were taken from a 3.2 μm ID nonlinear waveguide incorporated into the device explained in Section 3. Input pulses were 5 ns (FWHM). In solution, the SiNc was concentrated to 3.25×10^{-4} mol/L and the waveguide was 1.8 cm long, which yielded a T_{linear} of 45% for this optical limiter. Light was focused in through the entrance optical flat using a 10X objective. The device was adjusted to yield maximum coupling efficiency into the waveguide.
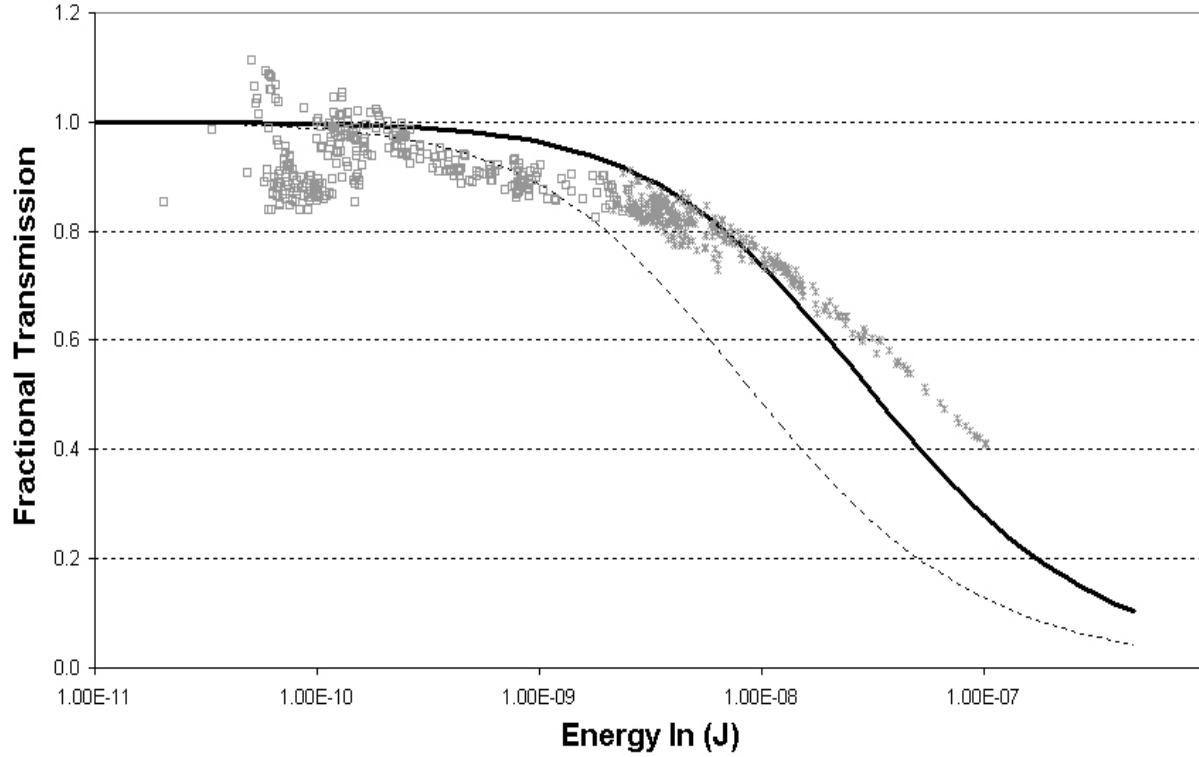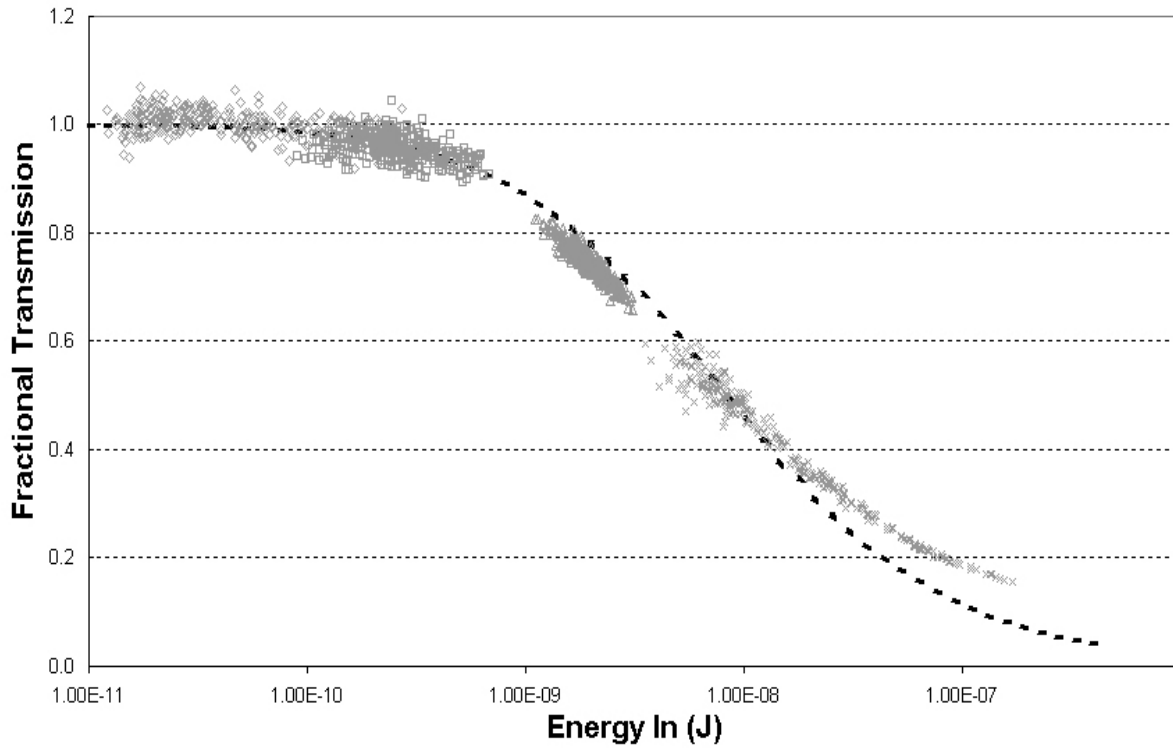
Figure 21: The relative transmission plot for a 3.2 μm nonlinear waveguide. Gray dots are the data and the dotted line is a simulation (effective core diameter = 3.2 μm).

10. Analysis of Multi-Mode Limiter Results

A. 200 μm (ID) Waveguide

The data presented above paint an interesting picture. As expected, the 200 μm data set (see Figure 17) coincides with its simulation quite well. The simulation parameters are: $\sigma_g = 2.3 \times 10^{-18}$ cm^2; $\sigma_e = 47.1 \times 10^{-18}$ cm^2; $R_0 = 100$ μm; $L_0 = 10$ cm; Tfwhm = 7 ns; SiNc molar concentration = 4.23×10^{-5} mol/L.

The 200 μm waveguide limited much like a free-space sample of similar concentration would (that is, if one could extend the Rayleigh Range to a length of 10cm). This occurs for a number of reasons. Firstly, the core diameter of this waveguide is so large that the number of modes that it supports approaches the continuum expected for a bulk material. The total number of confined modes, M, can be found approximately using the relationship

$$M \approx V^2/2. \qquad\qquad (52)$$

For this waveguide, $M \approx 47,000$. Secondly, light funneling into the waveguide's core (via the commercial fiber optic) enters the waveguide with an already extremely multi-modal energy distribution. The input pulses spread throughout the entire transverse area of the core as they propagate through the SiNc solution. The waveguide's length of 10 cm further reinforces this phenomenon—the longer a fiber waveguide is, the more energy different modes can share during propagation.[10] The pulses, by stimulating a large number of allowable modes in the core, are allowed to propagate through the core with a wide Gaussian spatial energy distribution. Thus, as expected, the 200 μm waveguide fits the simulation quite well.

B. 75 μm (ID) Waveguide

The 75 μm nonlinear waveguide, on the other hand, tells a much different story (see Figure 18). In this case, the 75 μm simulation predicts a limiting response much less effective

than 75 μm waveguide actually produces. The parameters for simulation are: $\sigma_g = 2.3 \times 10^{-18}$ cm^2; $\sigma_e = 47.1 \times 10^{-18}$ cm^2; $R_0 = 37.5$ μm; $L_0 = 1.17$ cm; Tfwhm = 7 ns; SiNc molar concentration = 5.81×10^{-5} mol/L. One possible explanation for this behavior is some type of mode channeling effect that confines the light to an effective area smaller than the actual area of the waveguide core. It is conceivable that, in this case, because the input commercial fiber optic had a relatively small diameter (~50 μm), the incident pulses stimulated relatively few modes upon entering the nonlinear waveguide's core. Also, because the nonlinear waveguide is so short (1.17 cm), there is not sufficient propagation distance for pulses to spread throughout the core as they propagate.[10] Light propagating into the 75 μm core stimulates only a few modes, creating an energy distribution near the center of the core. These few modes may be a small fraction of the total number of allowed modes that this fiber is calculated to support (M ≈ 6650). As a result, because light pulses propagate as more intense packets restricted to the center of the core, the waveguide limits better than the simulation would indicate.

In effect, the waveguide demonstrates a smaller diameter (smaller than 75 μm). The solid-line plot in Figure 18 is a simulation of a nonlinear waveguide having a core diameter of 35 μm. The simulation parameters are: $\sigma_g = 2.3 \times 10^{-18}$ cm^2; $\sigma_e = 47.1 \times 10^{-18}$ cm^2; $R_0 = 17.5$ μm; $L_0 = 1.17$ cm; Tfwhm = 7 ns; SiNc molar concentration = 5.81×10^{-5} mol/L. This simulation fits the actual data more closely. Thus, the propagating light pulses confine their spatial extents to a radius of ~ 18 μm (measured from the waveguide's transmission axis). The 75 μm waveguide acts like a 35 μm waveguide.

C. 10 μm (ID) Waveguide

Figure 19 shows the data taken from the 10 μm nonlinear waveguide. Data were acquired from this waveguide using the device explained in Section 3. Adjusting the 10X input

objective to maximize the coupling efficiency into the core of the waveguide ensures that only

the modes close to the transmission axis are stimulated. Based upon the results achieved with

the 75 μm waveguide, it is expected that the 10 μm waveguide will limit better than a simulation

of a 10 μm waveguide would predict.

The solid-line plot in Figure 19 represents a simulation of a 10 μm nonlinear waveguide's

limiting response. In this case, the total number of allowed modes is $M \approx 120$. As is very

apparent in the plot, the nonlinear waveguide begins limiting light earlier than the simulation

predicts; the actual data show that the optical limiter began limiting against pulse energies of $\sim$

100 pJ, the simulation does not begin to limit until pulse energies of $\sim$ 1 nJ. This order-of-

magnitude discrepancy can be explained by the mode channeling effect. The simulation

parameters for the 10 μm simulation are: $\sigma_g = 2.3 \times 10^{-18}$ cm^2; $\sigma = 47.1 \times 10^{-18}$ cm^2; $R_0 = 10$ μm;

$L_0 = 1.8$ cm; Tfwhm = 7 ns; SiNc molar concentration = 3.25×10^{-4} mol/L.

Again, simulating smaller core diameters can help to estimate the effective diameter of

the 10 μm waveguide's core. The dotted-line plot in Figure 19 is a simulation of a 3.4 μm

nonlinear waveguide—it fits the data almost exactly. The simulation parameters are:

$\sigma_g = 2.3 \times 10^{-18}$ cm^2; $\sigma = 47.1 \times 10^{-18}$ cm^2; $R_0 = 3.4$ μm; $L_0 = 1.8$ cm; Tfwhm = 7 ns; SiNc molar

concentration = 3.25×10^{-4} mol/L. Thus, a good approximate value for the diameter of the mode

channel created in the 10 μm waveguide's core is $\sim$ 3.4 μm.

D. 6.3 μm (ID) Waveguide

Figure 20 shows data collected from a 6.3 μm nonlinear waveguide. It should be

mentioned that these data were taken at the US Naval Academy (whereas the other data were

taken at the Naval Research Laboratory) using a different laser (which created 5 ns pulses

(FWHM)) and a different set of energy meters. It was very difficult to electromagnetically

isolate the energy sensors, and the readings at low energies proved very noisy (as is quite apparent in Figure 20).

A 5 ns incident pulsewidth should not provoke a limiting effect as easily as a 7 ns pulsewidth. Indeed, as the data demonstrate, a 5 ns pulse does not induce as marked a limiting effect, and the waveguide actually begins to limit at approximately the same energy-per-pulse that the 10 μm waveguide does (the 10 μm waveguide was investigated using 7 ns pulses). However, this effect alone cannot explain the observed behavior. The 6.3 μm waveguide produces an unexpected response. Apparently, the mode channeling effect observed in the 75 and 10 μm waveguides is only partially demonstrated in the 6.3 μm waveguide. As the waveguide begins to limit, it does demonstrate a smaller effective core diameter—it fits the 3.4 μm simulation for low input energies (this simulation is given by the dotted line in Figure 20). However, as the input pulses become more energetic, the waveguide's response stops demonstrating the mode-channeling effect, and the data begin to fit a 6.3 μm simulation (the solid line in Figure 20). The jump from the 3.4 μm simulation to the 6.3 μm simulation begins to occur for input energies of ~ 1 nJ.

The behavior of the 6.3 μm waveguide is difficult to explain. In this case, the core diameter is so small that the total number of allowed modes is $M \approx 45$. The waveguide's core-cladding boundary conditions may be playing a significant role in the waveguide's response. One possible explanation is that because so few modes exist within the core, as input energy increases beyond 1 nJ, the nonlinear response of the core forces a redistribution of propagating light energy to the perimeter of the core. Thus, an smaller effective core diameter is observed for low input energies, but this effect dies as the energy-per-pulse rises above 1 nJ.

For the 6.3 μm simulation, parameters are: σ_g = 2.3 x 10^{-18} cm^2; σ_e = 33.6 x 10^{-18} cm^2;

R_0 = 3.15 μm; L_0 = 1.8 cm; Tfwhm = 5 ns; SiNc molar concentration = 3.25 x 10^{-4} mol/L. For

the 3.4 μm simulation, parameters are: σ_g = 2.3 x 10^{-18} cm^2; σ_e = 33.6 x 10^{-18} cm^2; R_0 = 1.7 μm;

L_0 = 1.8 cm; Tfwhm = 5 ns; SiNc molar concentration = 3.25 x 10^{-4} mol/L.

E. 3.2 μm (ID) Waveguide

Figure 21 presents the data produced by a 3.2 μm nonlinear waveguide. These data were

also taken at the US Naval Academy. At the time these were taken, the energy sensors used to

collect the data had been sufficiently isolated from electromagnetic noise; these data are much

less noisy than the 6.3 μm waveguide's data.

It is so difficult to couple into a 3.2 μm core (it might take hours to adjust the apparatus to

couple light into the core) that trying to stimulate any given set of modes becomes an act of

futility. Also, within this 3.2 μm core, few modes exist (M = 12). Most of the remaining

allowable low-order modes distribute energy toward the perimeter of the core. Thus, it is a safe

assumption that the 3.2 μm waveguide will not demonstrate any mode channeling effect.

As expected, the data do not indicate any mode channeling effect. The data in Figure 21

coincide very closely to the 3.2 μm simulation (the dotted-line plot in the Figure 21). The

simulation parameters are: σ_g = 2.3 x 10^{-18} cm^2; σ_e = 33.6 x 10^{-18} cm^2; R_0 = 1.6 μm; L_0 = 1.8 cm;

Tfwhm = 5 ns; SiNc molar concentration = 3.25 x 10^{-4} mol/L.

11. The Single-Mode Optical Limiter

From the inception of this project, one of the main goals was to create and test a single-mode nonlinear waveguide. To our knowledge, this has never before been accomplished. The idea was that the single-mode waveguide optical limiter could potentially limit against input pulse energies drastically lower than multi-mode waveguide limiters.

In a multi-mode waveguide, stimulated modes can transfer energy amongst one another. The implication is that the mode field may redistribute energy so as to minimize the fluence that any part of the core experiences. This redistribution acts to minimize the amount of limiting that the core can achieve. However, in a single-mode waveguide, only one mode exists. Therefore, this mode cannot distribute energy into other modes. It can only carry energy through the core with an approximately Gaussian distribution, holding most of its energy near the center of the core as it propagates.

Furthermore, if the core of a single-mode nonlinear waveguide is composed of a strongly absorbing RSA material (like SiNc), then the core will preferentially limit the most intense portion of the incident pulse (the center). Because the lowest-order mode may only propagate with an approximately Gaussian energy distribution, then limiting in the center of the pulse's energy distribution may have repercussions throughout the rest of the distribution. Our theory predicts that the most intense limiting effect, which is created at the center of the pulse, will flatten the rest of the of the allowed Gaussian energy distribution, forcing much of the propagating energy to be lost out the sides of the waveguide's core.

The discussed energy redistribution was easily observed in some of the multi-mode nonlinear waveguides. Perhaps the best example, the 6.3 μm nonlinear waveguide clearly

demonstrates modal energy redistribution as the energy-per-pulse made incident upon the core

was increased (see Figure 22).
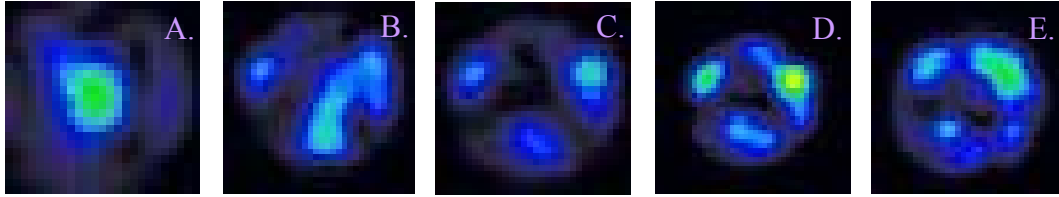
Figure 22: Energy distribution images from the output end of the 6.3 μm nonlinear waveguide's core. The pulse energy that creates image A is ~ 200 pJ and most of the energy is concentrated in the center of the core. The pulse energy that forms image B is ~ 900 pJ. At 900 pJ per input pulse, the propagating light is energetic enough to stimulate a nonlinear response from the waveguide. Image B shows that the waveguide's nonlinear response begins redistributing energy among the modes. The redistribution forces energy to distribute more evenly throughout the entire area of the core. The redistribution becomes more radical in C. (3 nJ per pulse), D. (19 nJ per pulse), and E. (260 nJ per pulse).

A successful single-mode optical limiter was not constructed until April of 2002. This single-mode device incorporates a 3.2 μm nonlinear waveguide into the same type of device explained in Section 3. An aluminum block, which is connected to a thermal control unit, sits in contact with the suspended capillary.

By raising the temperature of the waveguide's core, the core's index of refraction begins to decrease. If the index of refraction of the core becomes low enough (relative to the cladding's index of refraction), the core will only allow the lowest order mode (J_0) to propagate. By observing the output energy distribution of a linear core for various core temperatures, the temperature the device would begin exhibiting only single-mode propagation was determined to be ~ 50 degrees Celsius. During experiments investigating the single-mode nonlinear waveguide, the capillary was held at this temperature.

       The single-mode limiter may also have another advantage over multi-mode designs. Since, in the single-mode waveguide, the core index of refraction so closely approaches the index of refraction of the cladding, nonlinear refractive-index changes can begin to have serious affects on the transmission characteristics of a nonlinear waveguide. For a core made of a SiNc solution, high-energy pulses can cause a negative refractive-index change. If the energy of the pulse is high enough, this nonlinear change may actually force the core to exhibit a lower refractive index than the cladding, resulting in the loss of any waveguiding (i.e. total internal reflection would cease).

12. **The Single-Mode Results**

The constructed single-mode nonlinear waveguide was able to limit light amazingly well. In fact, the waveguide's limiting response initiated so early that, for the energies stimulating the nonlinear response, the signal-to-noise ratio was too low for the energy sensors to detect. At this point, it seems that the single-mode limiter initiates its nonlinear response against input pulse

A.
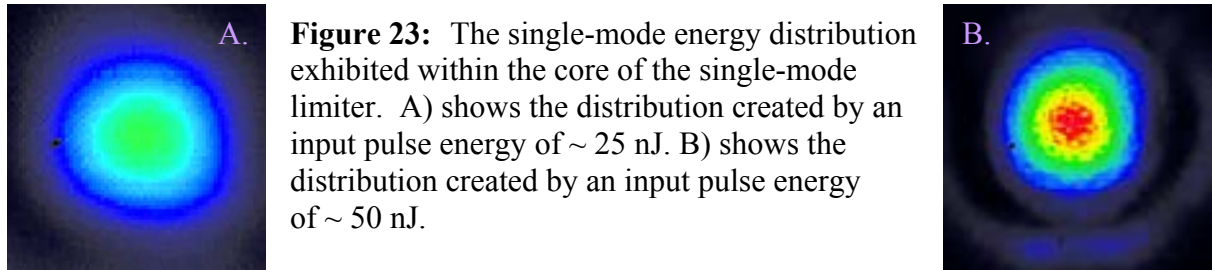
Figure 23: The single-mode energy distribution exhibited within the core of the single-mode limiter. A) shows the distribution created by an input pulse energy of ~ 25 nJ. B) shows the distribution created by an input pulse energy of ~ 50 nJ.

B.

energies somewhere below 20 pJ per pulse (a full order of magnitude earlier than the 3.2 μm multi-mode nonlinear waveguide). Unfortunately, because the energy sensors could not sense energies low enough to detect the waveguide's nonlinear shift, there is currently no way to plot the waveguide's transmission characteristics. In future, this problem may be solved by employing photo-multiplier tubes to amplify the waveguide's output energy.

Regardless of the difficulty in producing a transmission plot for the single-mode waveguide, core images were produced for various input energies-per-pulse (see Figure 23). These images show that the waveguide remains single-mode for all input energies-per-pulse. Building a single-mode waveguide optical limiter is an achievable feat. It produces a limiting response far more effective than any of the multi-mode waveguide optical limiters constructed in this project.

13. Conclusions and Future Work

This project has certainly demonstrated that nonlinear waveguide optical limiters are an effective means with which to limit light. To our knowledge, the limiting exhibited by some of the SiNc waveguides (the 10 μm waveguide and the single-mode waveguide in particular) far surpasses the limiting response achieved by SiNc in any previous experiments. And, to be sure, the waveguide geometry proves a very effective tool when building an optical limiter

The data presented above also reaffirm the validity of the SiNc's well documented effective three-level model. Using this three-level model as the basis for simulations, the simulations (when mode channeling was taken into effect) created quite accurate facsimiles of the real data. This computer simulation cannot accurately model the response of the single-mode limiter. Building a model that accounts for core-cladding boundary conditions is a future goal.

The data have also shown the sensitivity that nonlinear waveguide limiting responses can demonstrate towards launch conditions (the way light is coupled into the core of a waveguide). It seems that in short 1.8 cm fiber segments, propagating pulses are not given enough time to spread their energies across a waveguide's entire modal field (given that only a few modes are stimulated to begin with). Another interesting finding, the energy distribution images taken of the 6.3 μm nonlinear waveguide explain how a small-diameter waveguide's modal field can redistribute energy if a nonlinear response is stimulated within the waveguide (see Figure 22).

Perhaps most importantly, this project has proven that a single-mode nonlinear limiting waveguide is a viable device. And, it has demonstrated that a single-mode limiter can limit light against extremely low energies. The core-cladding boundary conditions within a fiber waveguide can reinforce a nonlinear core's ability to limit light.

In future experiments, heavy emphasis will be placed on refining the single-mode waveguide limiter. Special steps will be taken to reduce noise from the experimental setup and more precise energy sensors will be employed to measure the nonlinear response of the single-mode limiter. Efforts to build a mathematical model for the single-mode limiter have already begun. Other future investigations will probe the limiting abilities of different nonlinear materials when housed within the cores of waveguides. Finally, nonlinear waveguides will be tested against different wavelengths, including infrared wavelengths used in most commercial fiber systems.

Bibliography

1. James S. Shirk, et. al., *Appl. Phys. Lett.* **63** (14), 1880-1882 (1993).

2. I.C. Khoo, *J. Opt. Soc. Am. B.* **15**, 1533-1540 (1998).

3. I.C. Khoo, *Chemical Physics.* **245**, 517-531 (1999).

4. Joseph W. Perry, et al., *Optics Letters.* **19**, 625-27 (1994).

5. David Griffiths, *Introduction to Electrodynamics*. (Prentice Hall, 1999).

6. Robert Eisberg, et. al. *Quantum Physics of Atoms, Molecules, Solids, Nuclei, and Particles*. (John Wiley and Sons, 1985).

7. Peter W. Milloni, *Lasers*. (John Wiley and Sons, 1988).

8. Eugene Hecht, *Optics*. (Addison-Wesley Publishing Co., 1987).

9. Gerd Keiser, *Optical Fiber Communications*. (McGraw-Hill, Inc., 1991).

10. J. Nathan Kutz, *Journal of Lightwave Technology*. **16**, 1195-1201 (1998).

Appendices

Appendix A: Fortran Model for a Three-Level Reverse-Saturable Absorber

```fortran
C This program computes an 1-D array of energy output vs. a similar 1-D array
C of energy input for a three level limiter (aka an excited state absorber).
C It treats the input beam as temporal and spatial gaussian.  This is a free space
C simulation and takes no account for boundary conditions provided by waveguide
C core and cladding indices of refraction.  Comments in this program indicate necessary
C input parameters for the 3 level limiter SINC.
C       The original form of this program was created by Ryan Lindle from NRL.
C He again revised the program 6/1/93.  Further modifications have been made by
C Midshipman JJ Wathen of the US Naval Academy for his Trident Project investigating
C nonlinear optical limiting within capillary waveguides.  His modifications were made
C in February of 2002.
C       Two more levels can be added by decommenting the relevant lines,
C     restoring the type definitions at the beginning
C     removing the statements that set G2 and R2=0
C     and changes in the input and output statements.
C Revised to correct radial distribution of the Gaussian beam
C Altered the array sizes to fit steps used better
C Varied the radial integration step size with r
c Incorporated the reflectivity corrections, print files
C   with and without these corrections
C Revised 6/30/95 J Shirk  Ver F2A has 50 energy steps
C
        IMPLICIT REAL*8 (A-Z)
        INTEGER I,J,K,IR,IZ,IT,II,IIN,M_flag,INC_DR
C Elements of arrays N0 and M0 indicate ground state population for various Ein, R, Z, T.
C Elements of arrays N1 and M1 indicate excited state population.
        DOUBLE PRECISION N0(60,200),N1(60,200)
        DOUBLE PRECISION M0(60,200),M1(60,200)
        DOUBLE PRECISION TRANS(100),I0(100),TRexp(100),Msum
        REAL*8 EIN(100)
        COMMON/XYZ/N0,N1,N2,N3,M0,M1,M2,M3,TRANS,I0,TRexp
c  Avogadro's number
        NA=6.022E23
c  Planck's constant/2 Pi
        HBAR=1.054E-34
c  Pi
        PI=4*ATAN(1.0)
c  Speed of Light
        C=3E8
        OPEN (UNIT=1,FILE='temp.dat',STATUS='UNKNOWN')
        OPEN (UNIT=2,FILE='texp.dat',STATUS='UNKNOWN')
```

```
        write (*,*) 'Enter WAVELENGTH (nm)  '
        READ(5,*) LAMDNM
c  Wavelength IN (m)
        LAMBDA=LAMDNM*1E-9
c  Pulsewidth (FWHM).  7E-9 is Tfwhm for Nd:YAG at NRL.
        Tfwhm=7E-9
C  Beam spot radius for capillary is the radius of the capillary.
        write (*,*) 'Enter SPOT RADIUS (TO 1/e) IN AIR (microns)  '
        READ(5,*) R0Mic
c  HW1/eM Spotsize in cm
        R0=R0mic*1e-4
        write (*,*) 'WAVELENGTH (um):',SNGL(LAMBDA)
        write (*,*) 'PULSEWIDTH (FWHM):',SNGL(Tfwhm)
        write (*,*) 'SPOTSIZE (HW1/EM):',SNGL(R0)
        Tp=Tfwhm/(2*SQRT(ALOG(2.0)))
c  Set initial Time. At t0, pulse has only contacted limiting material
c  for ~.281 ns nanoseconds.
        t0=-2.5*Tp
c Set the # of radial steps
        Ir=60
C  Set the initial radial step size to .05 R0
        dr=R0*.05
C y will start at dr and be stepped by dr for the radial integration
C   dr will vary in the radial integration loop to maintain power
c   (i.e. small dr near center of beam, large dr at the perimeter of the wavefront)
C ** Input Sample parameters **********************************
        write (*,*) 'Enter SAMPLE THICKNESS (cm)  '
c        L0=1.8 cm
        READ(5,*) L0
c        Convert thickness to cm
c        L0=L0*1e-4.
        write(*,*) 'INPUT--Ground state cross section  '
        READ (5,*) XS0
        write (*,*) 'INPUT--MOLARITY(MOLES/LITER)  '
        READ (5,*) MOLARITY
c        MOLARITY=2.63E-4 mol/L for SINC in 1.8 cm sample at 45% T
c        XS0 for SINC = 2.26E-18 cm^2
c        XS1 for SINC = 45E-18 cm^2
c        Here, we calculate the A0, the linear coefficient of absorption.
c        It is the XS0*DENSITY (DENSITY is basically the initial population in
c        the ground state).
        DENSITY=NA*MOLARITY/1000
        ALPHA=XS0*DENSITY
        A0=alpha
        write (*,*) ' N0=',density,' Alpha=',ALPHA
        write (*,*) 'INPUT EXCITED STATE CROSSSECTION--X1   '
```

```
      READ (5,*) XS1
      XS2=0
C Set the number of z steps to one step for every .005 increment in initial abs
C It might be necessary to increase this for strong RSA materials
C For strongly absorbing samples this gives alot of Z steps. It can be reduced
      Iz=10+IFIX(200.0*SNGL(ALPHA*L0))
c Iz is the number of z steps
      dz=L0/Iz
      write (*,*) 'No of z steps ',Iz,'z step size=',dz*1e4,' microns'
      write (*,*) 'No of r steps ',Ir,'r step size=',dr*1e4,' microns'
c Photon Energy
      hw=2*PI*HBAR*C/LAMBDA
      write (*,*)'hw=',hw,' J/photon '
C AREA is an approximate 1/e spot area
      AREA=PI*R0*R0
      write (*,*) 'laser spot area (1/e)= ',AREA,' cm2 '
C      write (*,*) 'INPUT--REFRACTIVE INDEX OF SAMPLE, SUBSTRATE  '
C      READ (5,*) N_SAMPLE,N_SUB
C Here we are accounting for reflectivity losses.  Because the data we are trying
C to model is already normalized, we do not need to account for reflective losses.
C Thus, we set the index of air equal to the index of the substance.
      N_SAMPLE=1.0
      N_SUB=1.0
c  Reflection calculation from the Refractive Indicies
      R_SAMPLE=((N_SAMPLE-1)/(N_SAMPLE+1))**2
      R_SUB=((N_SUB-1)/(N_SUB+1))**2
      R_INT=((N_SAMPLE-N_SUB)/(N_SAMPLE+N_SUB))**2
      REFL=(1-R_SAMPLE)*(1-R_SUB)*(1-R_INT)
      write (*,*) ' REFLECTION LOSS=',REFL
C      write (*,*) 'INPUT Upper state Lifetime --T1  '
C      READ (5,*) T1
C Here we enter the lifetime of the first excited state.  We are approximating it
c as being "long."  This is an effective lifetime because SINC is actually a five level
c model.  T1 is the effective lifetime of the first excited singlet and triplet states
c combined.
      T1=37E-9
c In this version lifetimes T2 and T3 are not used.
c Lifetime of the second excited state is "short."
      T2=1e-9
      T3=T2
      Tmin=Tp
      IF(T1.LT.Tmin) Tmin=T1
C      IF(T2.LT.Tmin) Tmin=T2
C      IF(T3.LT.Tmin) Tmin=T3
c As defined previously, Tp is approximately blah (Tfwhm/2*sqrt(alog(2))). T1 is obviously
c bigger than this.  In the next calculation, Tmin is set to 0.1*the shortest characteristic
```

```
c time (i.e., .1*Tp). The new Tmin is used below to determine the time steps
        Tmin=Tmin/10
c  Fsat is the saturation fluence (Gconst in the original program)
        Fsat=hw/XS0
        II=0
99     write (*,*) ' INPUT INITIAL INCIDENT ENERGY   '
        READ (5,*) E0
        IF(E0.EQ.0) GO TO 9123
C The initial energy is E0, it will be incremented by dE for IIN steps
        dE=1.2
        IIN=60
        write (6,1600)  N,A0,exp(-A0*L0)
C Write the initial data out to file
        WRITE(1,1100) LAMBDA,ALPHA,REFL
        WRITE(1,1200) XS0,XS1,exp(-A0*L0)
        WRITE(1,1300) T1,T2,T3
        WRITE(2,1100) MOLARITY,ALPHA
        WRITE(2,1200) XS0,XS1
        WRITE(2,1300) T1,T2,T3
C
**** Intensity Loop *****************************************************
        DO 600 II=1,IIN
C  The peak incident intensity, I0, is the energy/ pi^(3/2)*tp*r0*r0
C      AREA has been defined as pi*r0*r0
        I0(II)=E0/(SQRT(Pi)*AREA*Tp)
        EIN(II)=E0
C ** Useful diagnostics that can be printed if desired
c       write (*,*) 'ENERGY=',E0
c       write (*,*) ' FLUENCE=',E0/AREA
c       write (*,*) ' FLUX=',I0(II)/hw
c       write (*,*) 'POWER=',I0(II)*AREA
c       write (*,*) 'INTENSITY=',I0(II)
**** Initialize concentrations in levels 0 and 1.
        DO 12 J=1,IR
         DO 11 K=1,IZ
          N0(J,K)=DENSITY
          M0(J,K)=DENSITY
          N1(J,K)=0.0
          M1(J,K)=0.0
11       CONTINUE
12       CONTINUE
C Compute the total concentration, which should remain constant
        N=N0(1,1)+N1(1,1)
c Initial Absorption Coeff.
        A0=XS0*N0(1,1)+XS1*N1(1,1)
**** Time integration ***********************************************
```

```fortran
C
C Statement 20 is the beginning of the time integration,
C   The loop end is near label 600
C I is index for the time integration,
C II is the current incident energy index
C
C   Initialize the incident and transmitted energy to zero
        E_TRANS=0
        E_INC=0
        Et=0.0
C Start time at t0=-2.5 tp
        t=t0
        I=0
20      I=I+1
C Compute the intensity at time t, the current time, ie. I(r=0,z=0,t=t)
        Ioot=I0(II)*EXP(-((t*t)/(tp*tp)))
c Set the time step to 0.1 *pulse width or the response time
c  Fsat/I is the absorber response time
        dt=Fsat/(10*Ioot)
        IF (Tmin.lt.dt) dt=Tmin
C
C**** Radial integration ************************************************
C
        EXC=I*0.5-IFIX(I*0.5)
c This is an EVEN/ODD Exchange Var. EXC is 0 for even I, 1 for odd I
C It is used to switch between loop beginning at 40 and that at 200 for
C the state population calculations.
C This allows the storage of the populations on the previous time step
C   On the initial pass I=1 so EXC=1
C
C **** Initilize variables which store results of the integration
C *Prot* sums the incident intensity*area
c       It is the Incident Power (J/sec) during the  Radial Integration
        Prot=0.0
C *Prlt* and *Pj* sum the transmitted  intensity*area
c  They are the transmitted Power (J/sec) during the  Radial Integration
        Prlt=0.0
        Pj=0.0
C
C ** y is the current radial coordinate. starts at .05*R0
C   the y=0 point has no differential area
C    y is incremented by dr at the end of the loop
        y=0.05*R0
C This integer helps size dr at large radii
        INC_DR=1
C
```

```
C ***** Here begins the loop for the radial integration
C
30     DO 400 J=1,IR
C Irot is the incident intensity at the current r and the current time
C Two variables: Iabs and Irzt carry the intensity as a fn(Z) at r and t
C They will be reduced by the transmission as z is incremented
        Irot=Ioot*EXP(-((y*y)/(R0*R0)))
        Iabs=Irot
        Irzt=Irot
c
**** Z integration *///*****************************************
40     DO 300 K=1,IZ
C
C Irzt contains the current intensity for this r and t as we move through z
C G is the no of photons/sec in the current cell * dt
        G=Irzt*dt/hw
c The program is written to go to 200 first
        IF(EXC.GT.0) GO TO 200
**** Level 0************************************************************
C This section is for the odd iterations in time (I index),
C the previous populations are found in M0 and M1 etc.
C
C Level 1 Generation Rate
C G1 = I*sigma*N*dt, the number of molecules leaving 1 in the time step
C
        G1=M0(J,K)*XS0*G
c Level 1 Relaxation Rate
        R1=M1(J,K)*dt/T1
C Check to make sure the populations do not drop below zero
        IF((G1-R1).GT.M0(J,K)) GO TO 110
C Otherwise store the population for the next iteration in N0(r(J),z(K))
        N0(J,K)=M0(J,K)+R1-G1
        GO TO 120
110    N0(J,K)=0
**** Level 1************************************************************
c Level 2 Generation Rate is set to zero for a three level model
120    G2=0
C 120    G2=M1(J,K)*XS1*G
c level 2  Relaxation Rate, set to zero here for the 3 level model
        R2=0
C       R2=M2(J,K)*dt/T2
C Check to make sure the populations do not drop below zero
        IF((G2+R1-G1-R2).GT.M1(J,K)) GO TO 130
        N1(J,K)=M1(J,K)+G1+R2-G2-R1
        GO TO 140
130    N1(J,K)=0
```

```
**** Level 2****************************************************************
140    continue
C Level 3 Generation Rate
C      G3=M2(J,K)*XS2*G
C      R3=M3(J,K)*dt/T3
Cc Level 3  Relaxation Rate
C      IF((G3+R2-G2-R3).GT.M2(J,K)) GO TO 150
C      N2(J,K)=M2(J,K)+G2+R3-G3-R2
C      GO TO 160
C150   N2(J,K)=0
**** Level 3****************************************************************
C160   IF((R3-G3).GT.M3(J,K)) GO TO 170
C      N3(J,K)=M3(J,K)+G3-R3
C      GO TO 180
C170   N3(J,K)=0
***************************************************************************
C Compute the absorbance in the current cell
180    ABS=(XS0*N0(J,K)+XS1*N1(J,K))*dz
c      WRITE(6,1500) N0(J,K),N1(J,K)
        GO TO 290
**** Level 0****************************************************************
C The initial iteration starts here
c Level 1 Generation Rate
200    G1=N0(J,K)*XS0*G
c Level 1  Relaxation Rate
        R1=N1(J,K)*dt/T1
C Do not let the population fall below zero
        IF((G1-R1).GT.N0(J,K)) GO TO 210
C Otherwise store the population for the next iteration in M0(r(J),z(K))
        M0(J,K)=N0(J,K)+R1-G1
        GO TO 220
210    M0(J,K)=0
**** Level 1****************************************************************
C Level 1, the first excited state, is depleted by pumping to state 2
c The Level 2 Generation Rate is set to zero for 3 level model
220    G2=0
c220    G2=N1(J,K)*XS1*G
c level 2  Relaxation Rate, set to zero for 3 level model
        R2=0
C      R2=N2(J,K)*dt/T2
C Make sure the population stays above zero
        IF((G2+R1-G1-R2).GT.N1(J,K)) GO TO 230
C Compute the population of state 1
        M1(J,K)=N1(J,K)+G1+R2-G2-R1
        GO TO 240
230    M1(J,K)=0
```

```
**** Level 2********************************************************************
240     Continue
C       G3=N2(J,K)*XS2*G
C Level 3 Generation Rate
C       R3=N3(J,K)*dt/T3
C Level 3  Relaxation Rate
C       IF((G3+R2-G2-R3).GT.N2(J,K)) GO TO 250
C       M2(J,K)=N2(J,K)+G2+R3-G3-R2
C       GO TO 260
C250    M2(J,K)=0
**** Level 3********************************************************************
C260    IF((R3-G3).GT.N3(J,K)) GO TO 270
C       M3(J,K)=N3(J,K)+G3-R3
C       GO TO 280
C270    M3(J,K)=0
********************************************************************************
C ABS is the absorbance= alpha*dz of the current radial cell
280     ABS=(XS0*M0(J,K)+XS1*M1(J,K))*dz
        Msum=M0(J,K)+M1(J,K)
c       WRITE(6,*) Msum
C ****This checks the number of molecules. revised for floating compare
        IF(Msum.GT.(1.02*N)) GO TO 281
        IF(Msum.LT.(0.98*N)) GO TO 281
        GO TO 290
281     write (6,1301) ((N-Msum)/N)
c  If the molecules count is off Set error flag and exit
        M_flag=1
        go to 9123
C The intensity in this cell, Irzt, is reduced by the absorbance
290     Irzt=Irzt*(1-ABS)
C The incident intensity for this cell is reduced by the abs
        Iabs=Iabs*EXP(-ABS)
300     CONTINUE
****End Z Integration***********************************************

C **** The area of the current radial cell  = 2*pi*r*dr
        da=2*pi*y*dr
C  Prot sums the incident intensity*area
c       It is the Incident Power (J/sec) on the current cell
        Prot=Prot+Irot*da
C  Prlt starts as zero, it sums the transmitted  intensity*area
c It is the transmitted Power (J/sec) during the  Radial Integration
        Prlt=Prlt+Irzt*da
C Pj is a second calculation of the transmitted powerduring the radial integration
        Pj=Pj+Iabs*da
C       TRANSMISSION OF the J-TH RADIAL COMPONENT is = Prlt/Prot
```

```
C       it is also = Pj/Prot
C**** Adjust the radial integration differential element size
C      This section trys to keep the incident power about constant
C
        IF(Y .LT. (0.11*R0)) THEN
          dr = .05*R0
        ELSE IF(Y .LT. (1.49*R0)) THEN
          dr = .025*R0
        ELSE
          dr= INC_DR*INC_DR*.05*R0
          INC_DR=INC_DR+1
        ENDIF
C **** Increment the radius by dr
        y=y+dr
400    CONTINUE
****End Radial Integration*******************************************
C  E_INC sums the total incident energy over time
        E_INC=E_INC+Prot*dt
c E_TRANS sums the total transmitted  energy over time
        E_TRANS=E_TRANS+Prlt*dt
c  E_t sums the total transmitted  energy computed from absorbances over time
        Et=Et+Pj*dt
C      write (*,*) ' ENERGY--TRANS=',E_TRANS,' INC=',E_INC,' et=',et
C      write (*,*) ' TIME=',t,' TRANS=',E_TRANS/E_INC,' t(exp)=',Et/E_inc
        t=t+dt
        IF (t.LE.(2.5*Tp)) GO TO 20
*****End Time Integration********************************************
C Compute the total transmission for this inncident energy using the two methods
        TRANS(II)=E_TRANS/E_INC
        TRexp(II)=Et/E_inc
        write (1,1302) II,EIN(II)/(1-R_SAMPLE),TRANS(II),REFL*TRANS(II)
        write (6,1302) II,EIN(II)/(1-R_SAMPLE),TRANS(II),REFL*TRANS(II)
        E0=E0*dE
600    CONTINUE
        go to 99
C*** LEVEL POPULATION for each level versus time is *NOT* written to file 'tmp.dat'.
9123   If(M_flag.EQ.1)  write (1,1301) ((N-Msum)/N)
        DO 700 I=1,IIN
c
C      WRITE(1,1400) I0(I)/(1-R_SAMPLE),REFL*TRANS(I)
        WRITE(2,1302) I,EIN(I),TRANS(I),TRexp(I)
700    CONTINUE
        CLOSE(1)
        CLOSE(2)
        write (*,*) 'OUTPUT FILES:TMP.DAT (REFLECTION CORR) & TEXP.DAT'
1100   FORMAT (' ','MOLARITY=',E9.2,' ALPHA=',E9.2,' Refl= ', E9.2)
```

```
1200   FORMAT (' ','XS0=',E9.2,2X,' XS1=',E9.2,2X,' Trans=',E9.2)
1300   FORMAT (' ','T1=',E9.2,2X,' T2=',E9.2,2X,' T3=',E9.2)
1301   FORMAT (' ','Molecule count diverging, Ratio=',E9.2)
1302   FORMAT (I6,E10.3,2F10.5)
1400   FORMAT (E10.3,2X,F10.5)
1500   FORMAT (5(E10.4,2X))
1600   FORMAT ('N=',E9.2,2X,'1/cm^3, abs=',E9.2,2X,'T=',F10.5)
       END
```

Appendix B: MathCAD Mode-Finding Program

$\lambda := .532 \qquad a := 1.5 \qquad n1 := 1.4860 \quad n2 := 1.482 \qquad neff := n2\,, n2 + 0.00001 \; .. \; n1$

$k1 := 2 \cdot n1 \cdot \dfrac{\pi}{\lambda} \qquad k2 := 2 \cdot n2 \cdot \dfrac{\pi}{\lambda} \qquad \beta(neff) := 2 \cdot neff \cdot \dfrac{\pi}{\lambda}$

$u(neff) := \sqrt{\left[k1^2 - (\beta(neff))^2 \right]} \qquad w(neff) := \sqrt{\left(\beta(neff)^2 - k2^2 \right)}$

$x(neff) := u(neff) \cdot a \qquad y(neff) := w(neff) \cdot a$

$c1(neff) := -1 \cdot u(neff) \cdot \dfrac{Jn(1, x(neff))}{J0(x(neff))} \qquad c2(neff) := -(1 \cdot w(neff)) \cdot \dfrac{Kn(1, y(neff))}{K0(y(neff))}$

$f(neff) := c1(neff) - c2(neff)$

$soln := root \; (\, f(neff)\,, neff\,)$

$soln =$
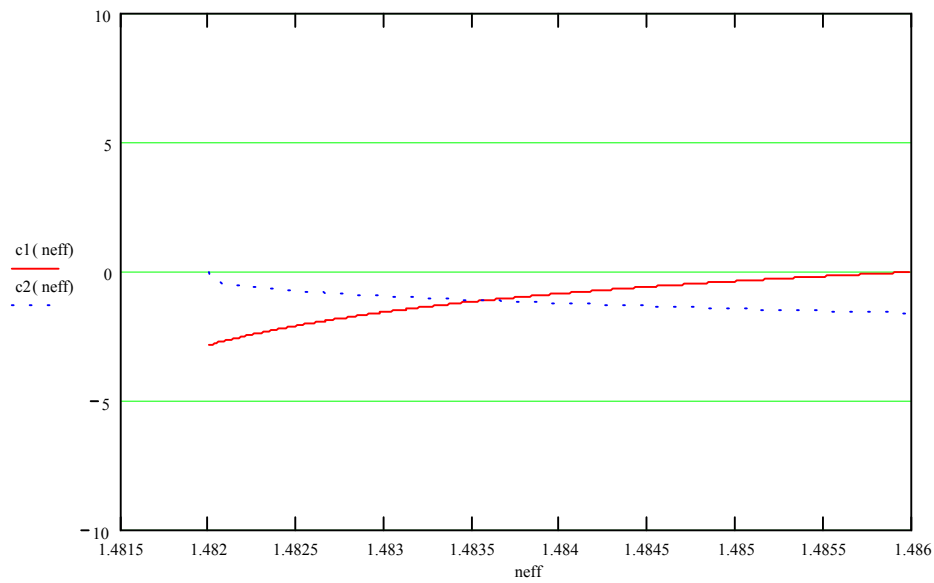
$V(n1, n2) := 2\,\pi \cdot \dfrac{a \cdot \sqrt{\left(n1^2 - n2^2\right)}}{\lambda}$

$V(n1, n2) = 1.93$